In vitro biological and in silico molecular docking and ADME studies of a substituted triazine-coordinated cadmium(II) ion: efficient cytotoxicity, apoptosis, genotoxicity, and nuclease-like activity plus binding affinity towards apoptosis-related proteins

Marzieh Anjomshoa, Mehdi Sahihi, Seyed Jamilaldin Fatemi, Shika Shayegan, Alireza Farsinejad, Bagher Amirheidari

In vitro biological and in silico molecular docking and ADME studies of a substituted triazine-coordinated cadmium(II) ion: efficient cytotoxicity, apoptosis, genotoxicity, and nuclease-like activity plus binding affinity towards apoptosis-related proteins

Marzieh Anjomshoa · Mehdi Sahihi · Seyed Jamilaldin Fatemi · Shika Shayegan · Alireza Farsinejad · Bagher Amirheidari

M. Anjomshoa (*) Pharmaceutical Sciences and Cosmetic Products Research Center, Kerman University of Medical Sciences, Kerman, Iran e-mail: anjomshoa_1014@yahoo.com M. Sahihi Roberval Laboratory, Université de Technologie de Compiègne, Alliance Sorbonne Université, Compiègne, France S. J. Fatemi Department of Chemistry, Shahid Bahonar University of Kerman, 76169-133 Kerman, Iran S. Shayegan Department of Pharmacy, Eastern Mediterranean University, TRNC via Mersin 10, Famagusta, Turkey A. Farsinejad Cell Therapy and Regenerative Medicine Comprehensive Center, Kerman University of Medical Sciences, Kerman, Iran B. Amirheidari Pharmaceutics Research Center, Institute of Neuropharmacology, Kerman University of Medical Sciences, Kerman, Iran B. Amirheidari (*) Department of Pharmaceutical Biotechnology, Faculty of Pharmacy, Kerman University of Medical Sciences, Kerman, Iran e-mail: b_amirheidari@kmu.ac.ir

Abstract A cadmium(II) complex containing dppt ligand with the formula [CdCl2(dppt)2], where dppt is 5,6-diphenyl-3-(2-pyridyl)-1,2,4-triazine was synthesized, elucidated and submitted to in vitro cytotoxicity studies against human breast (MCF-7), glioblastoma (U-87), and lung (A549) cancer cell lines as well as mouse embryo normal cell line (NIH/3T3), in comparison with cisplatin employing MTT assay over 24 and 48 h. The complex exhibited the highest cytotoxic efect against MCF-7 cells among the other three cell lines with IC50 values of 8.7±0.5 (24 h) and 1.2±0.7 μM (48 h). Signifcantly, fow cytometric assessment of the complex-treated MCF-7 and U-87 cells demonstrated a dose-dependent induced apoptotic cell death. The cellular morphological changes were in concord with cytotoxicity and fow cytometric results. The results of comet assay showed that the complex is able to induce DNA damage in MCF-7 cells. These observations are of importance, as sustained damage to cellular DNA could lead to apoptotic cell death. The results of DNA-binding studies indicated that the complex fts into the DNA minor groove and interacts with DNA via a partial intercalation. Moreover, the complex was able to efciently cleave pUC19 DNA through a hydrolytic mechanism. The binding afnity between the complex and apoptosis-relevant protein targets including APAF1, Bax, Bcl-2, Cas3, Cas7, and Cas9 was evaluated through molecular docking studies. In silico virtual studies revealed the complex's strong afnity towards apoptosis-related proteins; therefore the complex can act as a potential apoptosis inducer. Physicochemical, pharmacokinetics, lipophilicity, druglikeness, and medicinal chemistry properties of the complex were also predicted through in silico absorption, distribution, metabolism and excretion studies. **Keywords** 1,2,4-Triazine · Apoptosis · Comet assay · DNA cleavage · Molecular docking · ADME studies **Introduction** The heavy metal cadmium (Cd) is a nonessential trace element in the human body and has no known special biological role (Ma et al. 2020). Moreover, cadmium is a famous environmental pollutant that adversely afects human health. Liver, kidneys, lungs, and cardiovascular, immune and nervous systems are the major biotargets of cadmium (Mlejnek et al. 2019). The International Agency for Research on Cancer (IARC) has categorized the cadmium ion as a human carcinogen (Ahamed et al. 2020). However, there are reports suggesting that coordination of the cadmium ion with organic molecules reduces its toxicity, indicating that organic molecules may have a modulative function by chelating the Cd(II) ion (Li et al. 2020). Therefore, for the biological activity of Cd (II), various complexes are investigated while for toxicity studies, the Cd ion itself is assessed (L'Azou et al. 2014; Ahamed et al. 2020). A wide variety of biological activities of Cd(II) complexes such as DNA binding

ability (Manikandan et al. 2013; Morgan et al. 2017; Alalawy et al. 2020), cytotoxicity (Guan et al. 2014; Fang et al. 2018; Tsave et al. 2019), genotoxicity (Khandar et al. 2019; Rukk et al. 2019), antibacterial (Korkmaz et al. 2014; Majumdar et al. 2018; Aljahdali and El-Sherif 2020; Gitarić et al. 2020; Zhang et al. 2020), antifungal (Korkmaz et al. 2014; Aljahdali and El-Sherif 2020; Gitarić et al. 2020), and antioxidant (Aljahdali and El-Sherif 2020) properties has come to the current research focus. The results of the past decade research on cadmium complexes, as potential anticancer drugs, are indicative of their cytotoxicity and induction of cell death via apoptosis (Luo et al. 2016; Zhang et al. 2017; Abyar et al. 2019; Khandar et al. 2019). In 2016, Li and coworkers synthesized a cadmium(II) complex coordinated to N-(1-phenyl-3-methyl-4-(4-chlorobenzoyl)- 5-pyrazolone)-2-thiophenecarboxylic acid Hydrazide and 1,10-phenanthroline ligands. They found this complex more cytotoxic to HeLa and Eca-109 cancer cells than cisplatin. Moreover, their results demonstrated that the complex can efectively induce the apoptosis in HeLa cells and cell cycle arrest at G0/ G1 phase (Luo et al. 2016). In 2019, Khandar et al. investigated DNA binding, cyto- and genotoxicity of a new cadmium(II) complex containing the 2-pyridinecarbaldehyde isonicotinoyl hydrazone ligand. They concluded that the Cd(II) complex binds with the calf thymus-DNA through intercalation. Their cytotoxicity results indicated that the complex has potent cytotoxic efects against A549 cells and induce cell death via apoptosis. The genotoxicity studies (DAPI staining and DNA fragmentation assays) confrmed the induction of apoptosis and nuclear dysfunction by the complex (Khandar et al. 2019). Khandar and co-workers also synthesized two new cadmium(II) complexes using N(4)-phenyl-2-formylpyridine thiosemicarbazone and 5-aminotetrazole ligands and evaluated their nephrotoxicity and cytotoxicity in vitro. They demonstrated that both complexes have cytotoxic efects on MCF-7, Caco-2, and cisplatin resistant A549 cancer cell lines, where both complexes induced apoptosis in a caspase-dependent way (Abyar et al. 2019). The naturally occurring 1,2,4-triazine and its derivatives are six-membered heterocyclic compounds containing three nitrogen atoms. These compounds are well-known for their signifcant biological and medicinal applications such as antiHIV, anticancer, antiinfammatory, antimalarial, antimicrobial, antileishmanial, and antiviral activities (Arshad et al. 2017; Cascioferro et al. 2017). The 5,6-diphenyl-3-(2-pyridyl)-1,2,4-triazine (dppt) (Scheme 1) is a 3,5,6-trisubstituted 1,2,4-triazine which contains two phenyl and one pyridyl rings attached to the core triazine ring (Machura et al. 2008; Yamada et al. 2015). Despite the widespread medicinal properties reported for the 1,2,4-triazine derivatives (Arshad

et al. 2017; Cascioferro et al. 2017 and frequent reports on the synthesis of their metal complexes (Machura et al. 2008; Ibrahim et al. 2011; Yamada et al. 2015; Zvirzdinaite et al. 2017), we found few reports addressing biological activities of such complexes containing dppt as ligand (Lopes et al. 2017; Bravo et al. 2019; Babgi et al. 2020). In 2017, Morais and Villa de Brito's group synthesized and investigated cytotoxicity of a Cu(I) complex of general formula [Cu(dppe)(dppt)]+, where dppe is 1,2-bis(diphenylphosphino) ethane. This complex displayed high cytotoxicity on the ovarian cisplatin sensitive A2780 and the breast MCF-7 human cancer cells. In the ovarian cells the complex rapidly induces production of ROS (reactive oxygen species) in a dosedependent manner probably through mitochondrial pathways (Lopes et al. 2017). In 2019, they synthesized and studied cytotoxicity of another Cu(I) complex, [Cu(dppf)(dppt)][BF4], where dppf is 1,10-bis(diphenylphosphino)ferrocene. Their results showed that the complex has high cytotoxicity in two human breast adenocarcinoma cell lines (MCF-7 and MDAMB231) (Bravo et al. 2019). In 2020, Babgi and co-workers prepared and evaluated DNA-binding and cytotoxicity of a copper(I) complex, [CuBr(dppt)(PPh3)]. The complex indicated good cytotoxic efects in PC-3, MOLT-4, and MCF-7 cancer cells due to the presence of nitrogen heteroatoms and more extended delocalized π-systems, as they concluded. In vitro DNA-binding studies demonstrated the complex can bind to DNA with Kb=14× 105 M−1 (Babgi et al. 2020). In continuation of our studies (Anjomshoa et al. 2014, 2015a, b) to provide further insights into the biological activity of dppt-based metal complexes, we herein synthesized a Cd(II) complex coordinated to dppt. The in vitro antitumor efects of the Cd(II) complex in comparison with cisplatin were investigated by MTT assay on three human carcinoma cell lines (MCF-7, U-87, and A549) and one noncancerous cell line (NIH/3T3). Apoptotic cell death mechanism was evaluated by fow cytometric analysis. DNA damage in MCF-7 cells was studied by comet assay. DNA-binding and plasmid DNA cleavage activity of the complex was investigated via spectroscopic experiments, gel electrophoresis and molecular docking assessments. The complex's afnity towards an array of apoptosis-relevant protein targets including APAF1, Bax, Bcl-2, Cas3, Cas7, and Cas9 was assessed in silico through molecular docking experiments. Finally, an array of structure–activity and structure–property related features including physicochemical, pharmacokinetics, lipophilicity, water solubility, drug-likeness, and medicinal chemistry characteristics of the complex and the dppt ligand were determined by in silico ADME studies using the web-based toolkit provided by the Swiss Institute of Bioinformatics.

Experimental section

Materials and instrumentations Ethidium bromide (EB) and 5,6-diphenyl-3-(2- pyridyl)-1,2,4-triazine (dppt) were purchased from Alfa Aesar and Sigma-Aldrich, respectively. Fish sperm (FS) DNA was bought from Acros. A stock solution of FS-DNA in Tris bufer (5 mM Tris, 50 mM NaCl) gave an A260/A280 ratio of 1.9, indicating it efectively free of contamination (Chen et al. 2019). Also, its concentration was determined by UV absorbance at 260 nm (ε=6600 M−1 cm−1) (Anjomshoa et al. 2015b). Annexin V-FITC/propidium iodide (PI) fuorescent detection kit was received from Miltenyi Biotec. Supercoiled pUC19 DNA was extracted from a fresh culture of Escherichia coli by Bio Basic EZ-10 Minipreps kit. Agarose gel (molecular biology grade) and 3-(4,5-dimethylthiazol-2-yl)- 2,5-diphenyltetrazolium bromide (MTT) were purchased from Sigma-Aldrich. GelRed and the EcoRI restriction enzyme were obtained from Biotium and Fisher Scientifc, respectively. Other chemical reagents were purchased from commercial sources and used without further purifcation. UV–visible and fuorescence emission spectra were recorded on an Optizen 3220 UV spectrophotometer (Mecasys, Republic of Korea) and a Varian Cary Eclipse spectrophotometer (Varian, USA), respectively. The absorbance of 96-well plates was recorded by a Synergy 2 multi-mode plate reader (BioTek, USA). The microscopic and fluorescence microscopic images of cells were obtained by an inverted (Micros, Austria) and fluorescence microscope (Nickon Eclipse Ti, Japan), respectively. And, apoptosis assays were performed by a CyFlow® Space flow cytometer (Sysmex flow cytometry, USA).

Synthesis of [CdCl2(dppt)2] complex With a slight modification to a previously reported method (Marandi et al. 2011), to an aqueous solution (ca. 5 mL) of CdCl2·H2O (1 mmol, 0.20 g) was added an ethanolic solution (ca. 5 mL) of dppt ligand (2 mmol, 0.62 g) dropwise. The reaction mixture was stirred for 12 h at room temperature. Afterward, precipitation was fltered and the resulting solid was washed with water, and diethyl ether to yield a yellow solid. For further purification, this dried solid was recrystallized by difusion of diethyl ether into a methanolic solution of the complex, which gave yellow crystals suitable for crystallography. Yield: 0.56 g (69%). Anal. calc. for C40H28CdCl2N8 (%) C, 59.77; H, 3.48; N, 13.93. Found C, 59.51; H, 3.25; N, 13.44. IR (ν/cm−1) 514 (m), 534 (m), 688–771 (s), 1009–1181 (w), 1217 (w), 1254 (w), 1299 (w), 1369 (s), 1393 (s), 1444 (s), 1506 (s), 1578 (m N=N), 1647 (m, C=N). UV–visible (H2O/DMSO) λmax/(nm) (εmax/L mol−1 cm−1) 240 (27,600), 282 (36,400), 320 (21,200).

Stability studies in aqueous solution To investigate the stability of the complex in aqueous DMSO, it was dissolved in an aqueous solution containing 5% DMSO at the concentration of 25 μM. The UV–Vis spectra were recorded in the range of 238–388 nm at different time intervals (up to 1 week). The solution was stored at room temperature between measurements.

Cell lines and culture conditions The cytotoxic effect of the complex was assayed against human breast (MCF-7), brain (U-87), and lung (A549) cancer cell lines and also mouse embryo normal cell line (NIH/3T3), which were obtained from the National Cell Bank of Pasture Institute, Tehran, Iran, under codes C135, C531, C137, and C156 respectively. These cells were grown as adherent monolayers in a complete medium consisting of Dulbecco's Modified Eagle's Medium (DMEM high glucose, Gibco) or Roswell Park Memorial Institute medium (RPMI 1640, Gibco) with 10% fetal bovine serum (FBS, Gibco) and 1% penicillin/streptomycin (Biosera) in an incubator at 37 °C with a humidified atmosphere composed of 5% CO2.

Cytotoxicity assessment All cells were seeded in 96-well plates at a density of 5000–10,000 cells/well and incubated in complete culture medium for 24 h to adhere. A stock solution of the complex was freshly prepared in DMSO and immediately diluted with the medium to the desired concentrations. Final concentrations of the complex and cisplatin were in the range of 2.5–160 μM for 24 h and 0.6–80 μM for 48 h experiments, wherein the extent of DMSO was always lower than 1.0% v/v. After 24 h, 100 μL of different concentrations of the complex, cisplatin (as the positive control), and equivolume amounts of DMSO (as vehicle control) were added to the cells and 100 μL of medium only was added to the control wells (as the negative control). After the desired treatment times, MTT dye (0.5 mg/mL) was added to each well. After 3 h of incubation, the medium was removed and 100 μL of DMSO was added to solubilize the formazan crystals. The absorbance of each well was then measured by a multi-mode plate reader microplate spectrophotometer at 570 nm. The IC50 values, the concentration at which 50% of the cells remained viable relative to the control, were calculated in GraphPad Prism software.

Morphological changes and apoptosis mechanism in cells For the cell morphological changes studies, approximately 2× 105 cells of MCF-7 and 3× 105 cells of U-87 were seeded in T25 flasks at 37 ºC in a 5% CO2 incubator for 24 h before treatment. Afterward, the cells were treated with near IC50 concentrations of the complex and medium only was added to the control cells. Following 24 h complex exposure, the micrographs of untreated and treated cells were taken

directly using an inverted microscope without staining. For apoptosis detection, after seeding and treating the cells for 24 h as above, untreated and treated cells were harvested by trypsin–EDTA solution and collected by centrifugation. Then cells were stained according to the manufacturer's instructions (Miltenyi Biotec). In brief, the cells were washed twice with 500 μL of the binding bufer (1×) and resuspended in 100 μL of the same bufer (1X). To this, 5 μL of Annexin V-FITC was added, mixed well and incubated for 15 min in the dark at room temperature. Then the cells were again washed twice with 500 μL of binding bufer (1×) and resuspended in 300 μL of the same bufer. Finally, 3 μL of PI solution was added and immediately analyzed by flow cytometry.

Comet assay MCF-7 cells (10× 104 cells/well) were seeded in 6-well plates and cultured overnight. Next day, MCF-7 cells were exposed with diferent concentrations of the complex (2.5, 5, and 10 μM) for 24 h. Afterwards, the cells were trypsinized and collected by centrifugation. The cells were resuspended into the PBS bufer containing 0.5% low melting point agarose and rapidly pipetted onto pre-coated slides with 1% normal melting point agarose and then covered with a cover slip. After incubation at 4 °C in the dark for 20 min, the slides without the cover slip were immersed in ice-cold lysis solution (2.5 M NaCl, 0.01 M Tris, 0.1 M EDTA, 1% Triton X-100, and 10% DMSO, pH 10.0) at 4 °C overnight. After lysing the cell membrane, the slides were immersed in an alkaline electrophoresis solution (300 mM NaOH and 1 mM EDTA, pH>13.0) at 4 °C for 20 min. Electrophoresis was performed in the same alkaline solution at 25 V and 300 mA for 25 min. The slides were neutralized with a Tris bufer (0.4 M Tris–HCl, pH 7.4) and stained with a DNA green viewer for 15 min in the dark and then washed twice in distilled water. Finally, the DNA images were visualized under a fuorescence microscope. About 70 comets were randomly investigated by CASP software to analyze the length of the comet tails. The percentage of DNA in the tail (DNA tail %) was used to evaluate the extent of DNA damage in cells.

Statistical analysis The results were illustrated using GraphPad Prism software (version 8.0.1, Graphpad Software Inc., La Jolla, CA). The values were obtained from at least three independent experiments and were represented as the mean±standard deviation (SD). The signifcance of diferences between groups was determined by one way ANOVA test. P values lower than 0.05 were defned as a signifcant diference.

DNA-binding affinity and mode The stock solution of FS-DNA was prepared in Tris bufer (5 mM Tris, 50 mM NaCl) and the stock solution of complex was prepared in DMSO and diluted by Tris

bufer. In UV–Vis absorption titration experiments, a 12 μM constant concentration of the complex was titrated with varying concentrations of FS-DNA (from 60 to 660 μM). First the UV–Vis spectrum of the complex was recorded in the wavelength range of 232 to 432 nm. Then after each addition of DNA, changes in spectrum were recorded. Corrections were done by subtracting the spectra of the same amounts of DNA in a blank solution. In assessing competitive DNA-affinity between the complex and EB, first the emission spectrum of DNA pre-treated with EB ([DNA]/[EB]=10) was recorded in the wavelength range of 550–700 nm after excitation at 520 nm. Then changes in the emission spectrum of DNA–EB were recorded after addition of increasing amounts of the complex (0.8 to 9.5 μM). In molecular docking studies of the complex and DNA, the crystal structure of DNA (PDB ID: 423D) with sequence d(ACCGACGTCGGT)2 was taken from the Brookhaven Protein Data Bank (http://www. rcsb.org/pdb) with the resolution of 1.60 Å. The molecular docking procedure was similar to protein docking studies that will be mentioned below.

Nuclease-like activity The ability of the complex for cleaving the supercoiled pUC19 DNA (2686 bp) was investigated by agarose gel electrophoresis. Briefly, pUC19 plasmid DNA was extracted and purified from a fresh culture of Escherichia coli. The complex was freshly dissolved in DMF and immediately diluted to the desired concentrations (10, 20, 40, 80, and 160 μM) with Tris buffer (10 mM Tris/10 mM NaCl, pH 7.2) and mixed with the pUC19 DNA (2686 bp). The EcoRI restriction enzyme was used to linearize pUC19 DNA in Tris buffer as control. These reaction mixtures were incubated at 37 °C for 1 h, mixed with DNA loading dye and GelRed (for staining DNA) and loaded onto 0.8% agarose gel in Tris-Acetic acid-EDTA (TAE 1X). Electrophoresis was run at 80 V for 90 min. After DNA migration, the gels were visualized in a Bio Rad Gel documentation system and photographed. Densitometry of the DNA bands hence formed was analyzed using the IMAGEJ software (Wayne Rasband, National Institutes of Health, USA).

Binding affinity towards apoptosis-related proteins by in silico molecular docking studies Molecular docking studies was performed to predict the interaction between the complex and proteins involved in apoptosis pathway such as APAF1, Bax, Bcl-2, Cas3, Cas7, and Cas9. The crystal structures of target proteins were taken from the Brookhaven Protein Data Bank (http://www.rcsb.org/pdb). The pdb fles were prepared by removing the water molecules and

adding the missing hydrogen atoms and Gasteiger charges. AutoDock 4.2.6 program was used to perform the fexible ligand docking with the implemented empirical free energy function and the Lamarckian Genetic Algorithm (Morris et al. 1998). Furthermore, the macromolecule input fles were optimized by adding the Gasteiger charges and using the AutoGrid to calculate grids. For fnding the most stable confguration of complex-target systems; twostep molecular dockings were done for all the targets: (i) a blind docking calculation was performed to fnd the binding site of the complex on the structure of the biomacromolecule; (ii) the grid box was placed on center of the binding site and a docking with 60 lattice points along X, Y, and Z axes was performed. Grid point spacing was set to 0.375 Å, to allow the complex to rotate freely. Two hundred fifty docking runs with 25,000,000 energy evaluations for all molecular docking calculations were executed.

ADME predictions ADME studies were performed by the web-based SwissADME, which is a new comprehensive tool run by the Molecular Modeling Group of the Swiss Institute of Bioinformatics (http://www.sib.swiss) (Daina et al. 2017a, b). The structures of the complex and ligand were drawn into the website's imbedded ChemAxon's Marvin JS and converted to the SMILES (simplifed molecular-input lineentry system) format: Cl[Cd]Cl.C1=CC=C(C=C1) C1=NN=C(N=C1C1=CC=CC=C1)C1=CC=CC =N1.C1=CC=C(C=C1)C1=NN=C(N=C1C1=CC=CC=C1)C1=CC=CC=N1 and C.C1=CC =C(C=C1)C1=NN=C(N=C1C1=CC=CC=C1)C1= CC=CC=N1, respectively. Then, their ADME properties were predicted. A bioavailability radar shape is depicted for rapid estimation of drug-likeness of the compound, wherein six physicochemical properties (lipophilicity, size, polarity, solubility, fexibility and saturation) are taken into account. Human intestinal absorption (HIA) of the complex and the ligand as well as their permeation via the blood–brain barrier (BBB) were also visualized via the given BOILEDEgg simulation model (Daina and Zoete 2016).

Results and discussion

Synthesis and characterization of the Cd(II)–dppt complex The Cd(II)–dppt complex was prepared by following a general methodology wherein the bidentate dppt ligand reacts with CdCl2·H2O in a 2:1 mol ratio to yield the Cd(II) complex (Scheme 1). The structure of the complex was proved by CHN, FT-IR, and UV–Vis as well as single-crystal X-ray crystallography to be matching with that published previously (Marandi et al. 2011). As shown in Fig. 1, the coordination geometry around Cd ion is [CdCl2N4], which can be described as distorted

octahedral comprising of two bidentate NN donor dppt ligands and two monodentate chloride anions at cis position.

Aqueous stability studies The UV–Vis absorbance spectrum of the Cd(II) complex in an aqueous solution containing 5% DMSO over 1 week is shown in Fig. S1 (in Supplementary File). The absorbance values of the solution do not show any intensity changes or shifts in the maximum wavelength over 48 h. Afterwards, a slight reduction in the absorbance (hypochromicity) is witnessed possibly due to formation of complex aggregates (Zhao et al. 2015; Li et al. 2015a). Nevertheless, no precipitation, turbidity or color change was observed after long storage at room temperature. These fndings suggest that the complex has adequate stability in aqueous media, allowing its further biological properties evaluation.

Scheme 1 Synthesis route of $[CdCl_2(dppt)_2]$

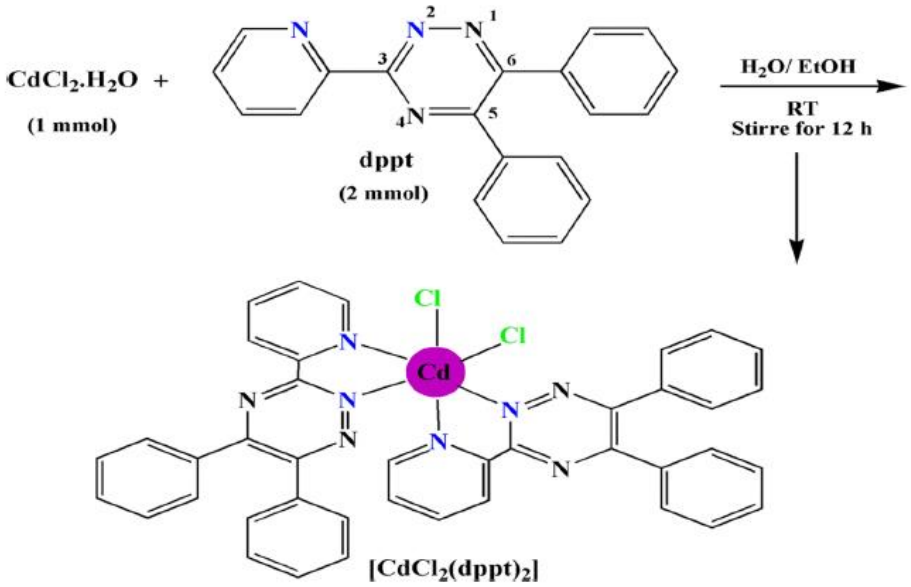

Cytotoxic efect of the complex by MTT assay The in vitro cytotoxicity of the Cd(II) complex was evaluated against MCF-7, U-87, A549, and NIH/3T3 cell lines by MTT colorimetric assay (Mosmann 1983) after 24 or 48 h treatment periods with incremental concentrations of the complex. Parallelly, cells treated with cisplatin, equivolume amounts of DMSO,

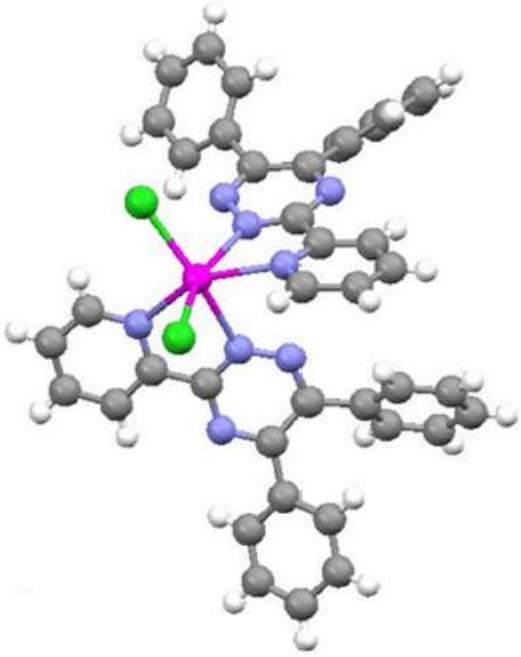

Fig. 1 The X-ray crystal structure of the Cd(II) complex, $[CdCl_2(dppt)_2]$. The structure is similar to that published previously (Marandi et al. 2011)

and medium only were used as a positive, vehicle, and negative control, respectively. Figures 2 and 3 represent the dose–response plots of cell viability (%) vs. diferent concentrations of the complex (μM) in the tested cell lines after 24 and 48 h exposure, respectively. The results show signifcant decrease in cell viability with increasing concentrations of the complex indicative of a concentration-dependent relationship. It is evident that the complex exhibits stronger cytotoxic efect in MCF-7 cells than the other cell lines, especially at 10 and 20 μM concentrations after 24 h of exposure (P values lower than 0.001 and 0.0001), which indicate the signifcant difference. The selectivity index (SI) of the complex was calculated as the ratio of its IC50 for NIH/3T3 cells over its IC50 towards the MCF-7 cells (Lopes et al. 2016; Ajibade et al. 2020). The SI values greater than 1 indicate that the compound is more toxic for the cancer cells; while the values less than 1 exhibit that the compound is more toxic to normal cells (Ajibade et al. 2020). Table 1 depicts the IC50 (μM) and SI values of the complex and cisplatin. High cytotoxicity and selectivity of the complex towards MCF-7 cells is confrmed by its values: IC50=8.7±0.5 μM and SI=2.4 over 24 h and IC50=1.2±0.7 μM and SI=3.2 over 48 h. Application of DMSO at equivolume amounts in these concentrations did not cause any observable cytotoxic efects in the vehicle control

experiments. Comparative cytotoxicity evaluations indicate that the complex shows a superior cytotoxic

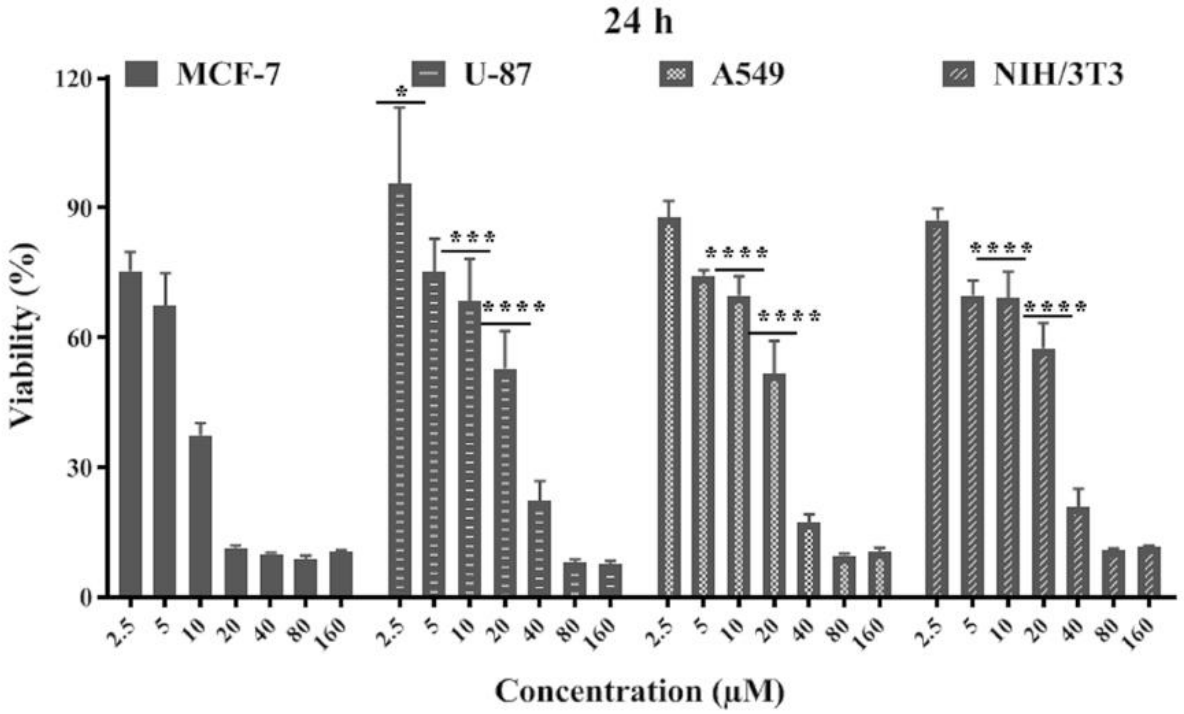

Fig. 2 Plots of viability (%) vs. concentration of the Cd(II) complex (2.5 to 160 μM) against MCF-7, U-87, A549, and NIH/3T3 cell lines after 24 h (n = 3). The significant difference of cytotoxicity at each concentration was statistically evaluated between MCF-7 cells and the other cell lines, $*p < 0.05$, $***p < 0.001$, and $****p < 0.0001$

effect to cisplatin (Table 1). Noteworthy, extension of the treatment time from 24 to 48 h strongly reduces the cell viability, indicating a time-dependent manner. The IC50 value found for the complex against MCF-7 (24 h) can be compared with those in our previous reports on other dppt-based metal complexes: [ZnCl2(dppt)2]=10.4 μM, [NiCl2(dppt)2]=13.0 μM, and [Cu(H2O)(dppt)2] 2+ =9.8 μM (Anjomshoa et al. 2014, 2015a, b).

Apoptosis studies by flow cytometry Breast cancer (BC) is the most life-threatening cause in women and Glioblastoma (GBM) is the most aggressive and common type of brain tumor especially amongst adults. In addition, these malignancies are the most leading causes of death worldwide (Bray et al. 2018; Bhaskaran et al. 2020). Despite the extensive eforts and widespread research; treatment of these cancer types remains a signifcant challenge. Development of metal-based agents may be a promising strategy for the treatment of BC and GBM. A deep comprehension of the cellular death mechanism could actively aid in the process of the rational

design of ideal therapeutic agents for BC and GBM therapy in the future. Considering these facts and resource shortage, we decided to choose MCF-7 and U-87 cell lines and 24 h time course for further evaluation of cell death mechanism. To prove whether the complex can induce apoptosis in MCF-7 and U-87, the cells were double-stained with Annexin V-FITC/PI and analyzed by fow cytometry. This dual staining method is a highly efective way to quantify the population of cells in four states of viable, early apoptotic, late apoptotic (secondary necrotic), and necrotic (Spel et al. 2013). Thus, the obtained dot plot is composed of four quadrants interpreted as: (i) Annexin V–/PI– quadrant, unstained viable cells with intact plasma membrane and no phospholipid phosphatidylserine (PS) translocation. (ii) Annexin V+/PI– quadrant, cells at the early apoptosis with PS-translocated membrane stained only by Annexin V-FITC. (iii) Annexin V+/PI+ quadrant, cells in the late apoptosis (secondary necrosis) with translocated PS and partially disintegrated plasma membrane exposing DNA to the intercalator PI,

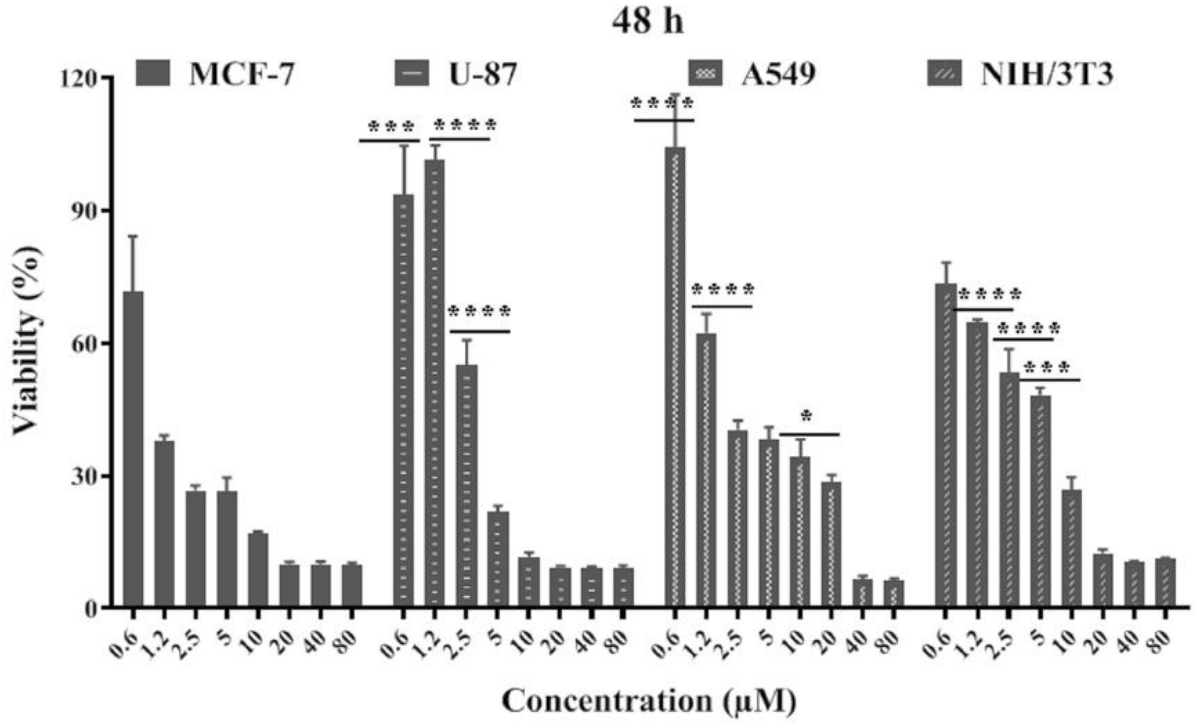

Fig. 3 Plots of viability (%) vs. concentration of the Cd(II) complex (0.6 to 80 µM) against MCF-7, U-87, A549, and NIH/3T3 after 48 h (n = 3). The significant difference of cytotoxicity at each concentration was statistically evaluated between MCF-7 cells and the other cell lines, ***$p < 0.001$ and ****$p < 0.0001$

Table 1 Cytotoxicity results of the Cd(II) complex and cisplatin against MCF-7, U-87, A549, and NIH/3T3 cell lines after 24 and 48 h incubation time

Compounds	IC_{50} (μM) ± SD				SI
	MCF-7	U-87	A549	NIH/3T3	
24 h					
Cd(II) complex[a]	8.7 ± 0.5	19.5 ± 3.6	18.2 ± 2.3	20.6 ± 1.8	2.4
Cisplatin[b]	23.0 ± 4.2	69.6 ± 3.6	50.9 ± 4.9	18.1 ± 3.0	
48 h					
Cd(II) complex[a]	1.2 ± 0.7	3.7 ± 0.2	4.0 ± 0.5	3.8 ± 0.4	3.2
Cisplatin[b]	11.6 ± 2.0	9.4 ± 0.2	12.8 ± 0.5	3.9 ± 0.01	

[a]The obtained IC_{50} values (μM) for the complex and cisplatin. The results are expressed as the mean ± SD (n = 3)

[b]The selectivity index (SI) was calculated for the MCF-7 cells: $SI = IC_{50}(NIH/3T3)/IC_{50}(MCF\text{-}7)$

[c]The final concentrations of the complex and cisplatin were in the range of 2.5 to 160 μM

[d]The final concentrations of the complex and cisplatin were in the range of 0.6 to 80 μM

stainable by both dies. And, (iv) Annexin V– /PI+ quadrant, cells at necrosis with total loss of cell membrane integrity but nucleic acid fragments still existing and interacting with PI (Spel et al. 2013). Figure 4 depicts fow cytometric results of MCF-7 cells treated by the complex (0, 5, 10, and 15 μM) for 24 h. Accordingly, the majority of the untreated cells (92.0%) are viable. When cells are exposed to 5 μM concentration of the complex, 11.23% of cells were found to have undergone apoptosis (6.77% early apoptosis and 4.46% late apoptosis), as compared to 6% of the control cells. Whereas with increasing the complex concentration to 10 and 15 μM, a decline in the population of viable cells and a signifcant increase in cells undergoing apoptosis was observed. The complex concentration of 10 μM raised totally the apoptotic population to 25.11% (12.03% early apoptosis and 13.08% late apoptosis) and at 15 μM concentration achieved 37.89% apoptosis rate (15.49% early apoptosis and 22.40% late apoptosis).

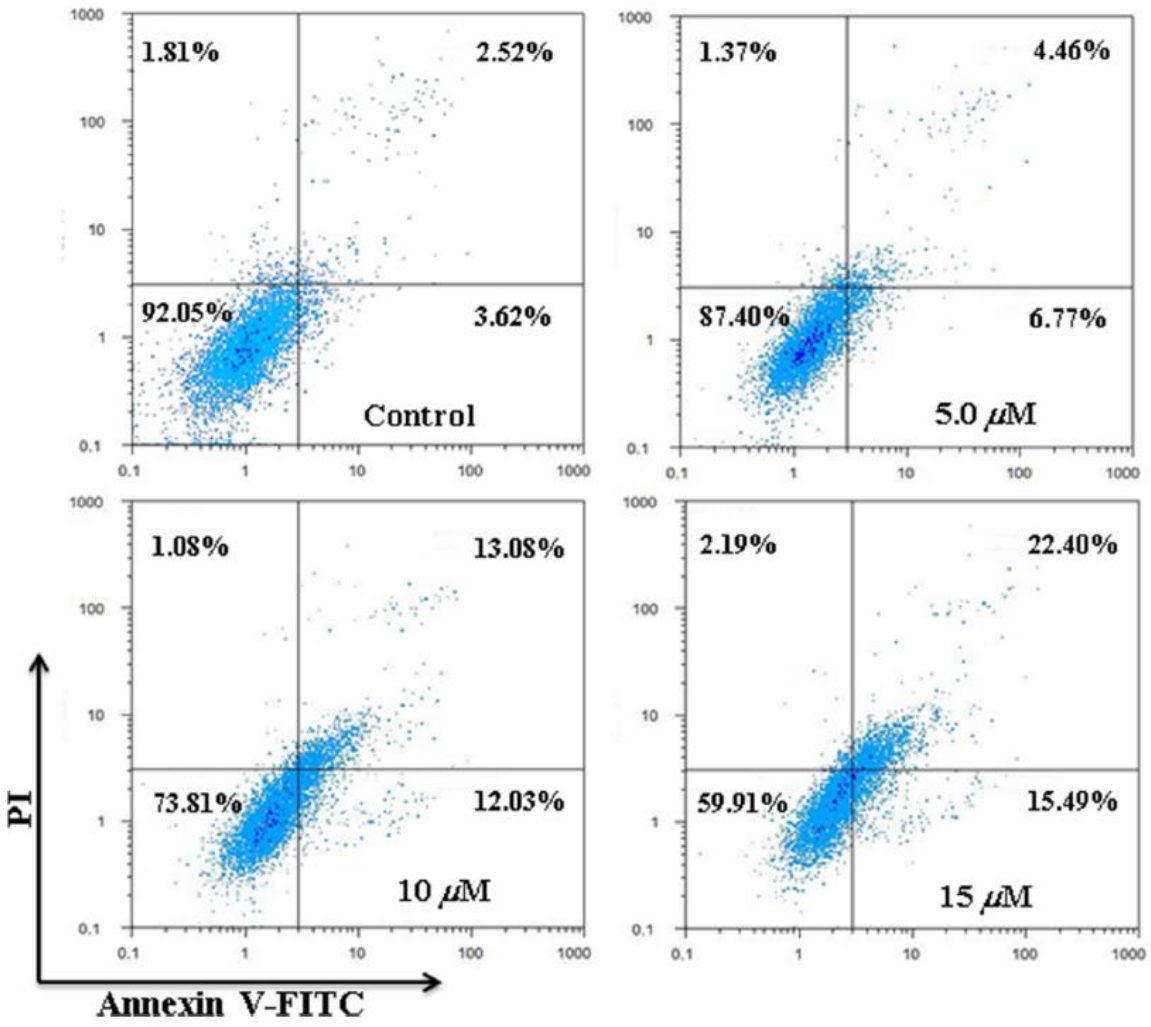

Fig. 4 Flow cytometric analysis of apoptosis detection (Annexin V/PI assay) in untreated and treated MCF-7 cells by the Cd(II) complex at the indicated concentrations (24 h)

Also, Fig. 5 shows flow cytometric results of the U-87 cells treated by complex (0, 5, 10, and 15 μM) after 24 h. In the control cells, 94.0% of the cells are viable and a total of 3.62% of cells are apoptotic. After the treatment of cells with 5 and 10 μM, no obvious changes in the percentage of the apoptotic cells were observed suggesting that the complex cannot efficiently induce apoptosis at low concentrations. However, upon increasing the complex concentration to 15 μM the apoptotic population is raised to 33.66% (5.73% early apoptosis and 27.93% late apoptosis). Table S1 (in supplementary file) exhibits flow cytometric results of MCF-7 and U-87 cells. Here again, our findings show a significant concentration dependent increase in the percentage of apoptotic cells. Interestingly, the complex induces a higher level of apoptosis in MCF-7 cells compared to U-87 cells at the same concentration

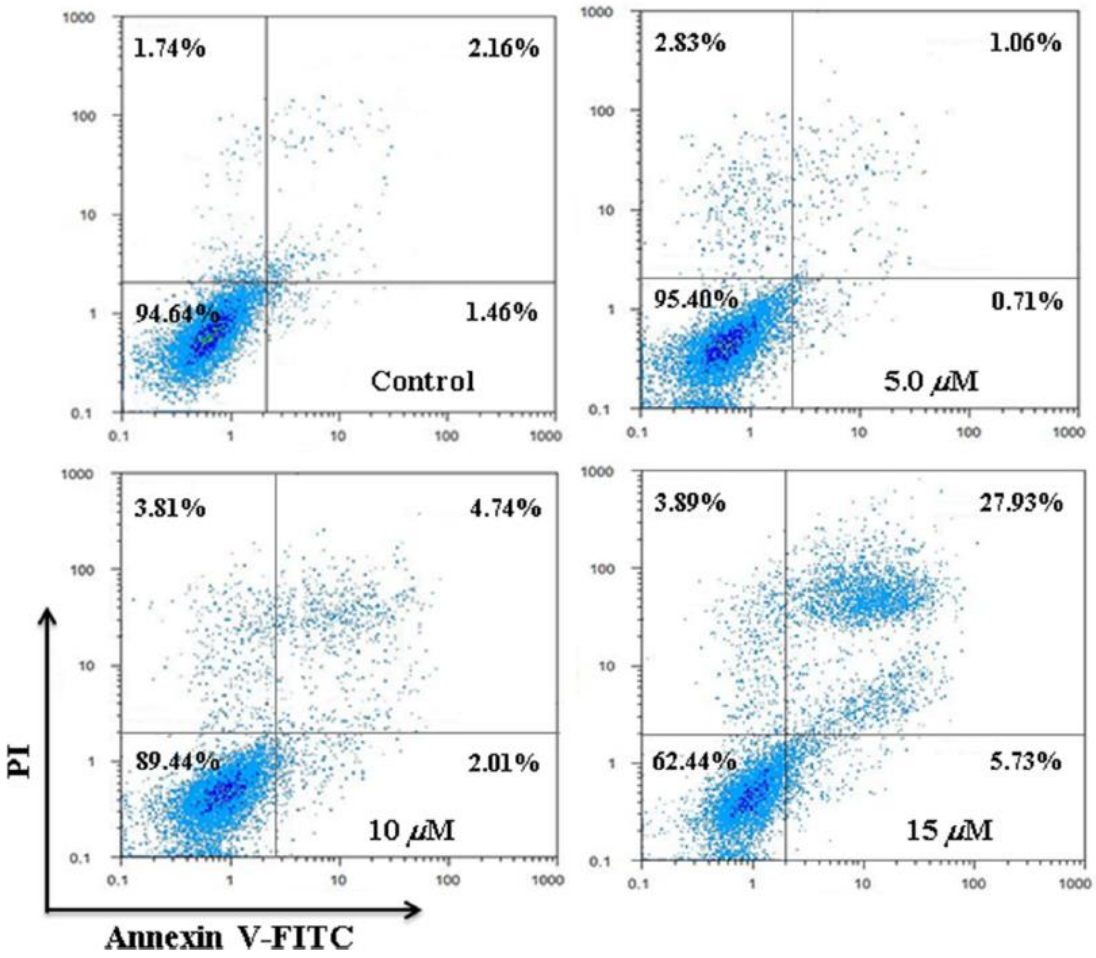

Fig. 5 Flow cytometric analysis of apoptosis detection (Annexin V/PI assay) in untreated and treated U-87 cells by the Cd(II) complex at the indicated concentrations (24 h)

Cellular morphological changes Morphological changes induced by the complex were directly photographed using an inverted microscope without any staining. Figures 6 and 7 depict the micrographs of MCF-7 and U-87 cells treated with the complex at indicated concentrations for 24 h, respectively. These images show that the untreated MCF-7 cells have a polygonal morphology, whereas increasing the complex concentrations (5 to 15 µM) induce observable gradual rounding of the cells. Furthermore, the number of foating dead cells increases along with increase of the complex concentration and resulting cause decrease of cell viability. Likewise, untreated U-87 cells have a polygonal morphology. The micrograph revealed that the increasing concentration of the complex up to 15 µM has led to a decrease of viable cells compared to control, which was confrmed by observing morphological changes especially cell rounding. These observations could be taken in close accordance with cytotoxicity and fow cytometric results.

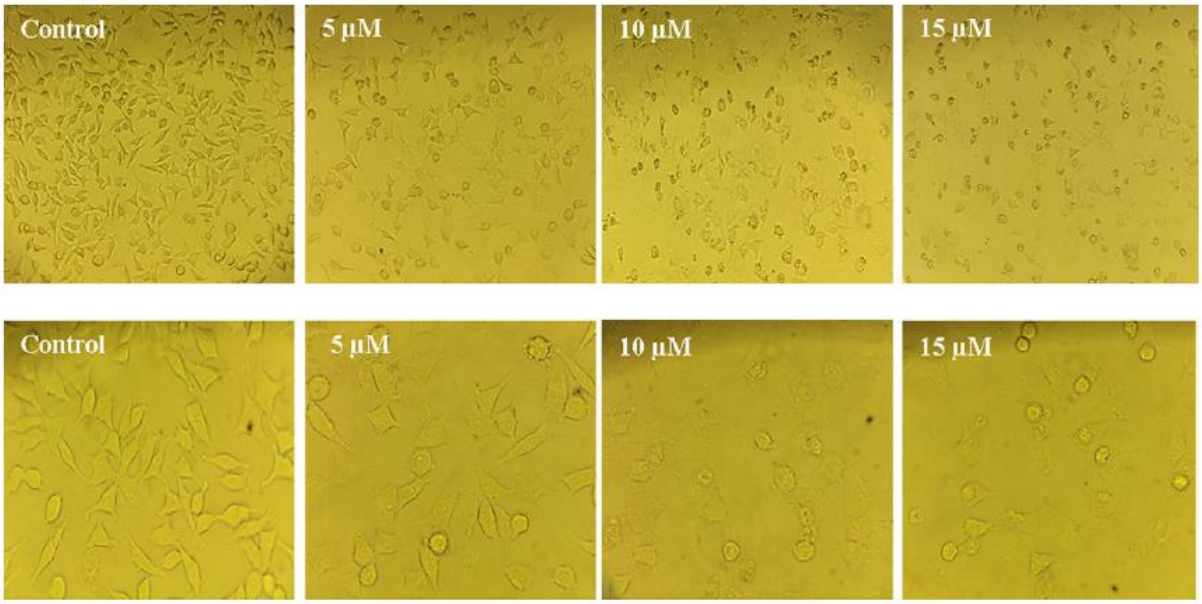

Fig. 6 Morphological analyses of MCF-7 cells after 24 h treatment by the Cd(II) complex. The upper and lower panels show microscopic photographs of cells at magnifications of 200X and 400X, respectively, in the absence (control) and presence of the indicated concentrations of the complex (indicated by the number inside each photo)

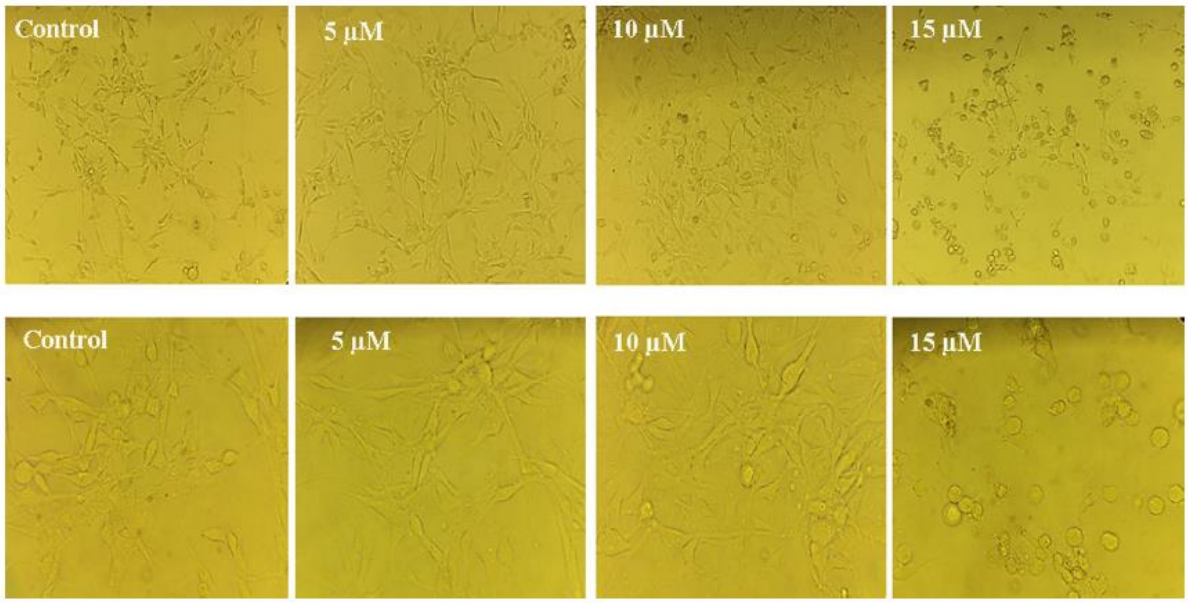

Fig. 7 Morphological analysis of U-87 cells after 24 h treatment by the Cd(II) complex. The upper and lower panels show microscopic photographs of cells at magnifications of 200X and 400X, respectively, in the absence (control) and presence of the indicated concentrations of the complex (indicated by the number inside each image)

Cellular DNA breakage by comet assay To achieve further insights into the induced DNA strand breaks in MCF-7 cells by the complex, the intracellular DNA damage was carried out using the

alkaline comet assay (single-cell gel electrophoresis) (Wang et al. 2020). In this assay, the resultant DNA images contain a head and tail which are called a comet. The comet head indicates the intact and unbroken DNA, while the comet tail indicates broken pieces of DNA as single and double-stranded DNA breaks (Matos et al. 2019). Therefore, the DNA tail (%) quantitatively refects the extent of cellular DNA damage. Figure 8A depicts comet-like appearance of DNA in untreated and the complex-treated MCF-7 cells. Moreover, Fig. 8B shows percentage of the DNA tail in untreated and the complex-treated MCF-7 cells. As seen in Fig. 8A, no comet-like form is observed in the untreated MCF-7 cells (control,) while the signifcant comet-like appearance appears in the complex-treated cells. When MCF-7 cells are exposed to 2.5 μM concentration of the complex for 24 h, 15% of DNA is found in the tail compared to untreated cells (2.9% of DNA in tail). Moreover, 24% of DNA is detected in the comet tail with increasing concentration of the complex to 10 μM, indicating a concentration-dependent DNA breakage. These results clearly indicate that the complex is able to induce cellular DNA damage, which is further evidence of apoptosis induction.

DNA-binding afnity and mode

UV–Visible spectral studies The absorption spectra of the complex in the absence and presence of increasing concentrations of FSDNA are shown in Fig. 9A. The UV–Vis spectrum of the complex demonstrates intense absorption bands at 240, 282, and 320 nm, which are assigned to the intraligand ($\pi \rightarrow \pi^*$) transitions of the coordinated dppt ligand (Anjomshoa et al. 2014, 2015a, b). At low concentrations of DNA (60 to 360 μM), no obvious changes in the spectrum are observed. While, upon increasing concentrations of DNA (420 to 660 μM), a hypochromism (as calculated by [Afree− Abound/ Afree]×100) at ~ 282 nm reaches as high as 14.0% at fnal DNA concentration and a bathochromic value of 4.0 nm (as calculated by $\Delta\lambda=\lambda bound-\lambda free$) were seen (Liu et al. 2015). These evident spectral changes indicate that the complex interacts with DNA via intercalation (Anjomshoa et al. 2019). Additionally, in order to quantitatively examine the binding strength of the complex with DNA, the value of the intrinsic DNA binding constant (Kb) was calculated by the ratio of the slope to the intercept in the plot of [DNA]/(εa − εb) vs. [DNA], according to equation S1 (Eq. S1 in Supplementary File) (Liu et al. 2015).

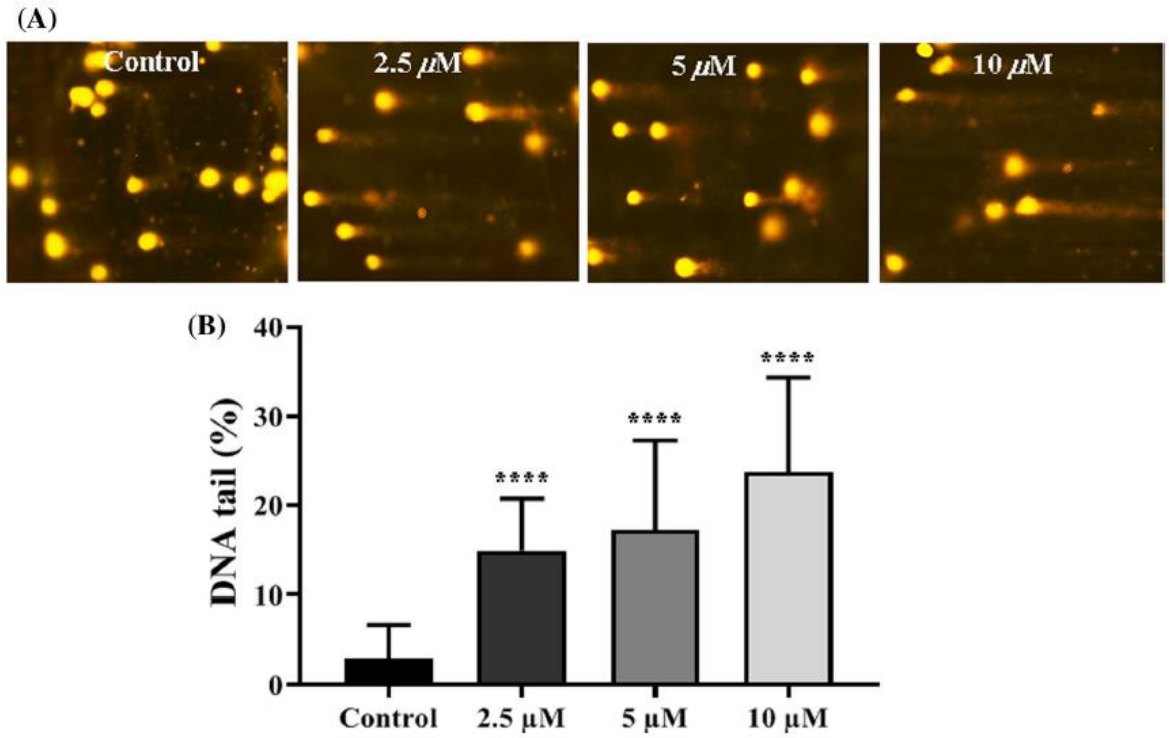

Fig. 8 **A** Detection of comet-like appearance of DNA in untreated and treated MCF-7 cells by the complex at indicated concentrations. **B** The corresponding DNA tail (%) in untreated and the complex-treated cells analyzed by CASP software, * represents a significant difference from the control group (p value < 0.0001)

The plot of [DNA]/(εa − εb) against [DNA] (Fig. 9A inset) also exhibits the two-phase binding curves. The measured Kb value of the complex is 0.15× 105 M−1, which suggests a moderate complexDNA binding afnity. This Kb is smaller than the values obtained for other dppt-based metal complexes (Kb=0.50× 105 M−1 (Anjomshoa et al. 2015b) and 1.97× 105 M−1 (Anjomshoa et al. 2014)) and/or similar to value obtained for dppt-based Ni(II) complex [Kb=0.10× 105 M−1 (Anjomshoa et al. 2015a)].

Competitive DNA-binding studies with ethidium bromide To achieve further insights into the binding mode between the complex and DNA, a well-accepted quenching assay based on the displacement of EB from EB-DNA composite was performed. Figure 9B represents the fuorescence quenching of EB-DNA system in the absence and the presence of increasing concentrations of the complex. Clearly, successive additions of the complex to DNA solution pretreated with EB caused very small reductions in the DNA-bound EB emission intensity. The extent of the decrease in the emission intensity correlates to the extent of displacement of the EB from the DNA structure (Jeyalakshmi et al. 2017; Martínez et al. 2017). The percentage of

quenching (as defned by %Q= [IEB-DNA − Ibound/IEB-DNA]×100) for this complex is approximately 13.0%. The EB displacement experiment indicates that the complex cannot efciently compete with EB to displace it from DNA conjugate. These results confrm that the interaction of the complex with DNA is diferent from EB. Besides, the quenching plot (Fig. 9B inset) revealed that the removal of EB from DNA-bound EB by the complex is in good agreement with the linear Stern–Volmer equation by using the equation S2 (Eq. S2 in Supplementary File). The KSV value calculated from the slope of the Stern–Volmer plot in our experiments is 0.16× 105 M−1, close to the dpptbased Zn complex, KSV =0.31× 105 M−1 (Anjomshoa et al. 2014) but much smaller than the values obtained for other dppt-based metal complexes, KSV =4.70× 105 M−1 (Anjomshoa et al. 2015b) and 8.80× 105 M−1 (Anjomshoa et al. 2015a).

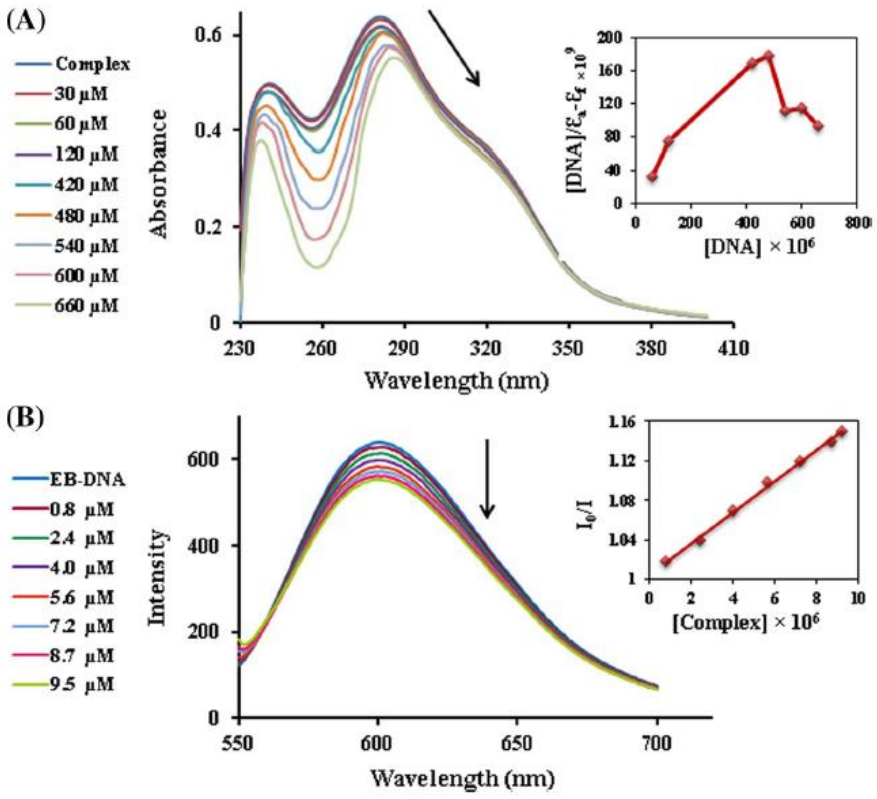

Fig. 9 **A** UV–Vis absorption spectra of the complex in the absence and the presence of increasing concentrations of DNA, [complex] = 12 µM and [DNA] = 30, 60, 120, 360, 420, 480, 540, 600, and 660 µM. Inset: plot of [DNA]/($\varepsilon_a - \varepsilon_b$) vs. [DNA]. **B** Emission spectra changes of the EB bound to DNA upon increasing concentration of the Cd(II) complex, [EB] = 1 µM, [DNA] = 10 µM, and [complex] = 0.8, 2.4, 4.0, 5.6, 7.2, 8.7, and 9.5 µM. Inset: plot of I_0/I vs. [complex]. The arrows indicate the direction of changes in the UV–Vis and emission spectra

DNA-binding studies by molecular docking In order to determine the binding mode and type of interactions between the complex and DNA, in silico studies was performed on a model DNA

duplex having the sequence d(ACCGACGTCGGT)2. Figure 10 visualizes the complex docked inside the binding site of DNA, revealing that the complex binds with the minor groove of DNA with standard binding free energy (ΔG°) of − 6.04 kcal mol−1 indicating a moderate binding afnity between the Cd(II) complex and DNA. The measured docking energy is routinely correlated to the docking cluster with maximum population and minimum binding free energy. This docking energy value is smaller than the value obtained for dppt-based Cu(II) complex, − 8.36 kcal mol−1 (Anjomshoa et al. 2015b). As shown in Fig. 10, hydrophobic bonds are the main interaction between the complex and DNA. These observations are in good agreement with the experimental results.

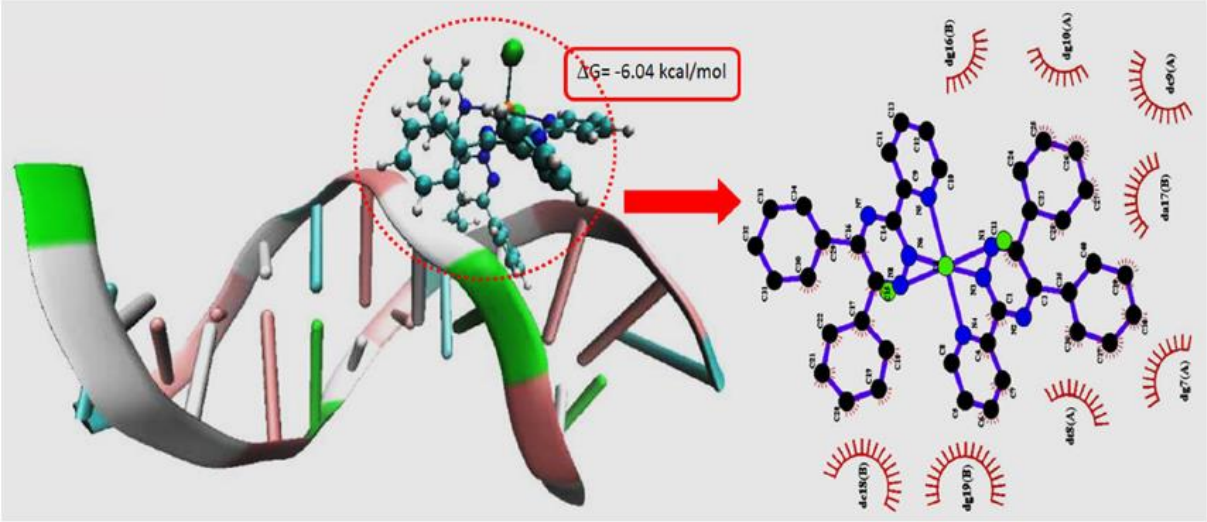

Fig. 10 The docked Cd(II) complex in the minor groove of model DNA with sequence d(ACCGACGTCGGT)$_2$ (PDB ID: 423D). Binding mode, type of interaction, and docking energy of the complex inside the binding site of DNA. Hydrophobic interactions are represented as red curves

Nuclease-like activity The in vitro interaction of the complex with circular plasmid DNA (pUC19 DNA) to assess its ability to cleave pDNA also was evaluated. The compact supercoiled plasmid DNA (form I or SC) is probably cleaved to single scission and/or double scission in the strands of the supercoiled plasmid to produce relaxed open-circular (form II or OC) and/or linear (form III or L). When plasmid DNA is subject to electrophoresis, the migration rate of these conformers is in the order of form I>form III>form II (Desbouis et al. 2012; Anjomshoa et al. 2019; Anjomshoa and Amirheidari 2022). Figure 11A shows gel-photograph obtained from hydrolytic cleavage activity of the complex treated with pUC19 DNA at 37 °C after 1 h incubation. The percentage of DNA forms were calculated according to the equations S3 to S5 (Eqs. S3 to S5 in Supplementary

File) from densitometric analysis. Figure 11B displays the corresponding histograms displaying the extent of DNA forms. The mean initial extent of SC, L, and OC forms in the control DNA is 83.0%, 1.0%, and 16.0%, respectively (Fig. 11A and B, lane control). Upon increasing concentrations of the complex from 10 to 160 μM (lanes 1–5), the amounts of L and OC forms increased gradually along with a decrease in SC form. For example, the extent of SC, L, and OC forms after exposure to the 80 μM concentration of the complex are 60.0%, 3.0%, and 37.0%, respectively. When pUC19 DNA was exposed to 160 μM concentration of the complex, the extent of SC, L, and OC forms are 49.0%, 4.0%, and 47.0%, respectively. These observations strongly support the complex's efcient capability to cleave DNA through the hydrolytic reaction pathway (Li et al. 2015b; Anjomshoa and Amirheidari 2022) in a concentration-dependent mode. It is noteworthy that a band corresponding to the linear form of DNA was observed after digestion of pUC19 DNA with EcoRI restriction enzyme (lane EcoRI) (Jin and Cowan 2005). In addition, control DNA with only DMF did not display any DNA cleavage under similar conditions (data not shown).

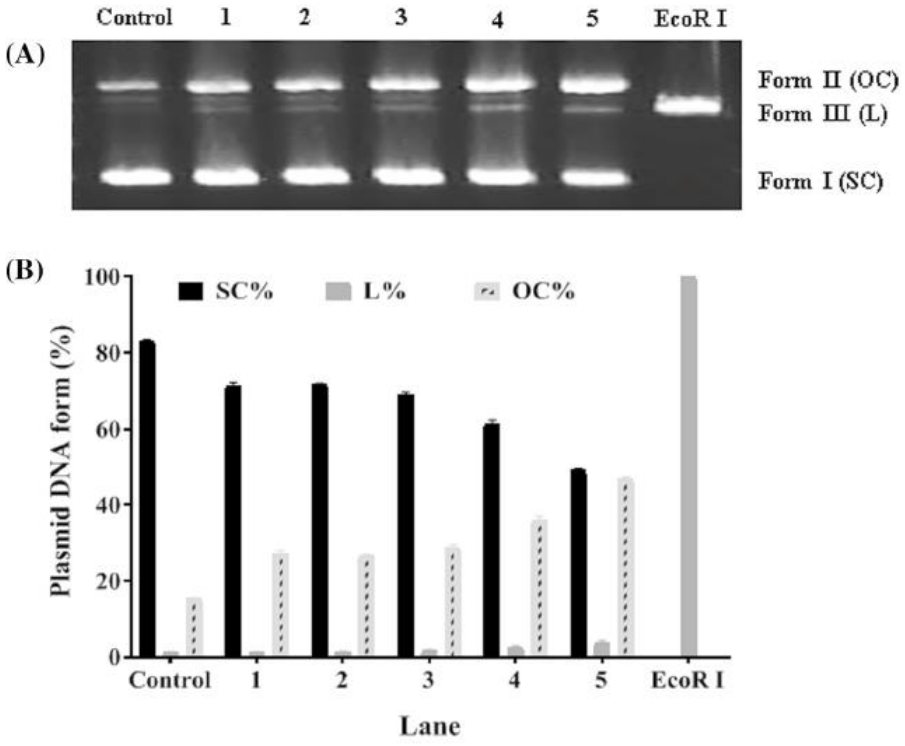

Fig. 11 **A** The hydrolytic cleavage of pUC19 (100 ng/μL, 37 °C, 1 h) by the complex. Lane control: pDNA alone; lane 1: pDNA + complex (10 μM); lane 2: pDNA + complex (20 μM); lane 3: pDNA + complex (40 μM); lane 4: pDNA + complex (80 μM); lane 5: pDNA + complex (160 μM); and lane *Eco*RI: pDNA + *Eco*RI restriction enzyme. **B** The extent of DNA forms from densitometric quantitative results analyzed by IMAGEJ software (n = 3)

In silico binding afnity towards apoptosis-related proteins It is of high interest to predict the molecular binding features of the complex with apoptotic proteins such as APAF1, Bax, Bcl-2, Cas3, Cas7, and Cas9 for further consideration. Molecular docking analysis is a reliable method to estimate the most stable structure of biomolecules—compound to understand the interaction details in drug discovery procedures (Mishra and Dey 2019). In order to fnd out the preferred location of the complex on proteins involved in apoptotic pathway, molecular docking studies were done by AutoDock 4.2.6 program. Figures 12 and 13 depict the binding mode and type of interaction of the complex with the proteins proposed to be involved in apoptosis phenomenon. Table 2 reports PDB ID and resolution of protein structure (Å) along with the molecular docking results containing the type of interaction, amino acids involved in interaction, and calculated binding energy scores (ΔG°, kcal/mol) between the complex and target proteins. The results show that hydrophobic interactions have the main role in the stability of the complex within the binding site of the targets. Moreover, there is one H-bond interaction between the N1 atom of the triazine

ring of one of the ligands with the hydroxyl of Tyr204 residue of Cas3 protein (Fig. 13). The docking energies are related to the docking cluster with maximum population of interacting residues and minimum binding free energy. According to the docking energies, afnity of the complex towards apoptosis-related proteins follow the order of Bcl-2>APAF1>Bax>Cas9>Cas3>C as7. As seen, the complex's afnity towards the antiapoptotic Bcl-2 protein is more favorable than the selected pro-apoptotic proteins. This strong interaction might cause inhibition and suppressing of Bcl-2 protein and fnally apoptotic cell death. This along with apoptosis results that the complex efciently enables to induce apoptosis in cells. These fndings are in close agreement with the docking results which were previously reported by Bhattacharyya and coworkers by using Molegro Virtual Docker (MVD 2010.4.0) software (Gogoi et al. 2019; Bhattacharyya et al. 2020; Dutta et al. 2020; Nath et al. 2020, 2021 Sharma et al. 2021). They studied the efect of Cu(II) and Co(II) complexes on anti-apoptotic Bcl-2 family proteins by in silico molecular docking as well as in vitro western blot experiments. Their docking results revealed that the complexes have high afnity towards Bcl-2 family proteins, resulting they are able to induce apoptosis through inhibition of anti-apoptotic Bcl-2 family proteins. These fndings were confrmed by western blot experiments (Nath et al. 2020). In other studies they investigated the in silico interaction between metal complexes and anti-apoptotic Bcl-2 family proteins. Their results demonstrated that the complexes have a high afnity towards Bcl-2 family proteins which lead to apoptotic cell death (Gogoi et al. 2019; Bhattacharyya et al. 2020; Dutta et al. 2020; Sharma et al. 2021; Nath et al. 2021).

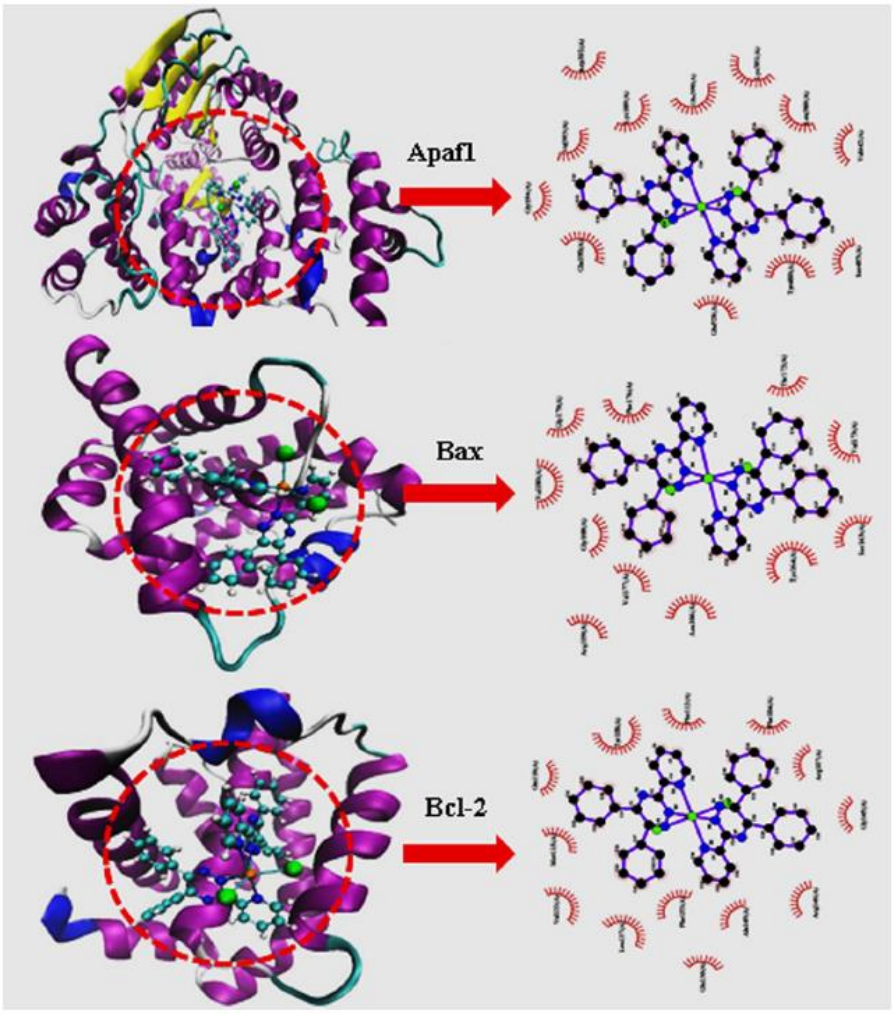

Fig. 12 Binding mode and type of interaction of the complex at the A-chain binding site of APAF1, Bax, and Bcl-2 proteins. Hydrophobic interactions are represented as red curves. (Color figure online)

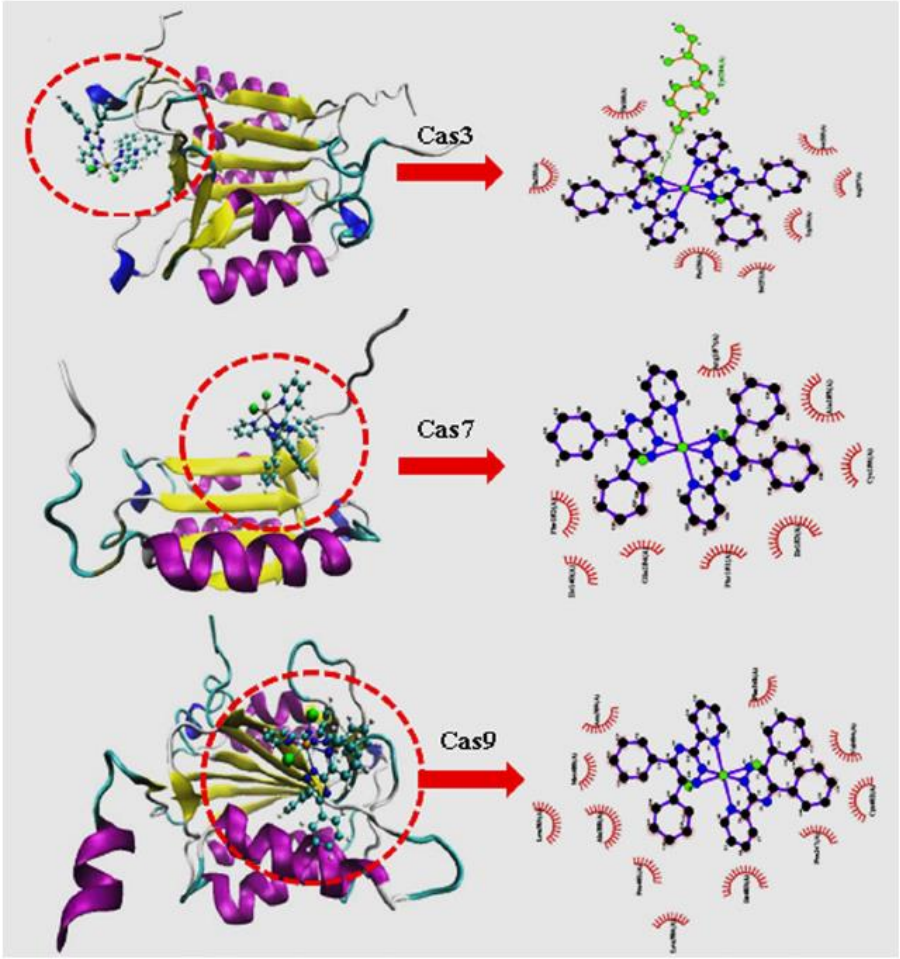

Fig. 13 Binding mode and type of interaction of the complex at the A-chain binding site of Cas3, Cas7, and Cas9 enzymes. Hydrophobic and H-bond interactions are represented as red curves and a green dotted line, respectively. (Color figure online)

Table 2 PDB ID and resolution of protein structure (Å), interaction type, amino acids of the A-chain binding site involved in interaction, and calculated binding energy scores (ΔG°, kcal/mol) between the complex and target proteins

Target protein	PDB, resolution (Å)	Interaction type	Amino acids involved in interaction	Binding energy (kcal/mol)
APAF1	1Z6T, 2.21	Hydrophobic	Gly194, Gln(190, 390), Glu528, Tyr489, Ser493, Val(442, 393), Leu389, Lys(391, 189), Asp392	− 9.09
Bax	4S0O, 1.90	Hydrophobic	Val(180, 177, 173), Gly(108, 179), Arg109, Asn106, Thr 172, Tyr164, Ser163, Phe176	− 9.06
Bcl-2	2XA0, 2.70	Hydrophobic	Val133, Leu137, Phe(153, 104, 112), Glu136, Ala149, Arg(146, 107), Gly145, Tyr108, Gln118, Met115	− 9.25
Cas3	5I9B, 1.80	Hydrophobic and H-bond interaction	Thr(255, 166), Phe256, Ser(251, 205), Trp206, Arg207	− 7.79
Cas7	3EDR, 2.45	Hydrophobic	Phe182, Ile(140,183), Gln184, Phe181, Cys186, Ala185, Arg187	− 7.57
Cas9	2AR9, 2.80	Hydrophobic	Leu(385, 384), Ala388, Pro(401, 247), Ile403, Cys402, Val404, Phe348, Asn389, Met400	− 8.26

ADME predictions A set of ADME-related properties of the complex as a whole and the dppt ligand were predicted by preliminary ADME studies. Table 3 represents the calculated parameters of the complex and the ligand. Figure 14 indicates a predicted BOILED-Egg diagram of the dppt ligand, from SwissADME web tool. BOILED-Egg model is a graphical diagram to predict gastrointestinal (GI) absorption (white ellipse) and/or BBB (yolk) (Daina and Zoete 2016). The number of rotatable bonds for the complex and the ligand are 6 and 3, respectively. The number of rotatable bonds is a parameter that determines fexibility (no more than nine rotatable bonds) (Daina et al. 2017a, b). Moreover, the number of hydrogen bond acceptors of the complex is 8. Topological Polar Surface Area (TPSA) value for the complex and the ligand is 103.12 and 51.56 Å2 , respectively. The value of TPSA below 140 Å2 reveals the efective transport of the compound inside the cellular plasma membrane (Qazi et al. 2018; Bojarska et al. 2020). Lipophilicity is determined by the partition coefcient between n-octanol and water (log Po/w). The value of consensus log Po/w, the mean of the values of fve available predictive models, is 5 and 3 for the complex and the ligand, respectively. These values also indicate good permeability inside the cellular membrane (Khan et al. 2018). The aqueous solubility of a compound is routinely predicted by three methods: ESOL, Ali, and SILICOS-IT. All of these methods calculate the log S values (defned as the logarithm of the molar solubility in water). Compounds are classifed according to their predicted solubility values in six categories: log S< −10=insoluble;−10< −6=poorly soluble;−6< −4=moderately soluble;−4< −2=soluble;−2 of in vivo studies or ultimately clinical trials, it will most probably have to be administered parenterally. ADME characteristics of the ligand alone, however, gave diferent features like high GI absorbability and well permeation via BBB, which was readily visualized by the BOILED-Egg model showing (Fig. 14). The complex could be introduced as a potential anticancer agent because it is not a p-glycoprotein (P-gp) substrate (Bojarska et al. 2020). The drug-likeness properties of the complex are compatible with the Veber rules. The complex and the ligand respectively have bioavailability scores of 0.17 and 0.55 (greater than zero), which means they possess signifcant biological activity in clinical trial stage (Fathima et al. 2018; Khan et al. 2018; Bojarska et al. 2020).

Table 3 In silico ADME properties of the complex and ligand

Parameter	Complex	Ligand	Parameter	Complex	Ligand
Physicochemical properties:			Pharmacokinetic		
Molecular weight (g/mol)	804.02	326.39	Gastrointestinal absorption	Low	High
Number of rotatable bonds	6	3	BBB permeant	No	Yes
Number of H-bond acceptors	8	4	P-gp substrate	No	Yes
Number of H-bond donors	–	–	CYP1A2 inhibitor	No	Yes
Molar refractivity	199.55	100.85	CYP2C19 inhibitor	No	Yes
TPSA (Å2)	103.12	51.56	Skin permeability coefficient (Kp in cm/s)	− 5.60	− 5.59
Liphophilicity			Drug-likeness		
Consensus Log Po/w	5.33	3.22	Veber	Yes	Yes
Water solubility			Bioavailability Score	0.17	0.55
Log S (ESOL)	− 10.10 (IS)	− 4.77 (MS)	Medicinal chemistry		
Log S (Ali)	− 9.91 (PS)	− 4.58 (MS)	Synthetic accessibility	4.77	3.32
Log S (SILICOS-IT)	− 8.44 (PS)	− 8.44 (PS)			

IS insoluble, *PS* poorly soluble, *MS* moderately soluble

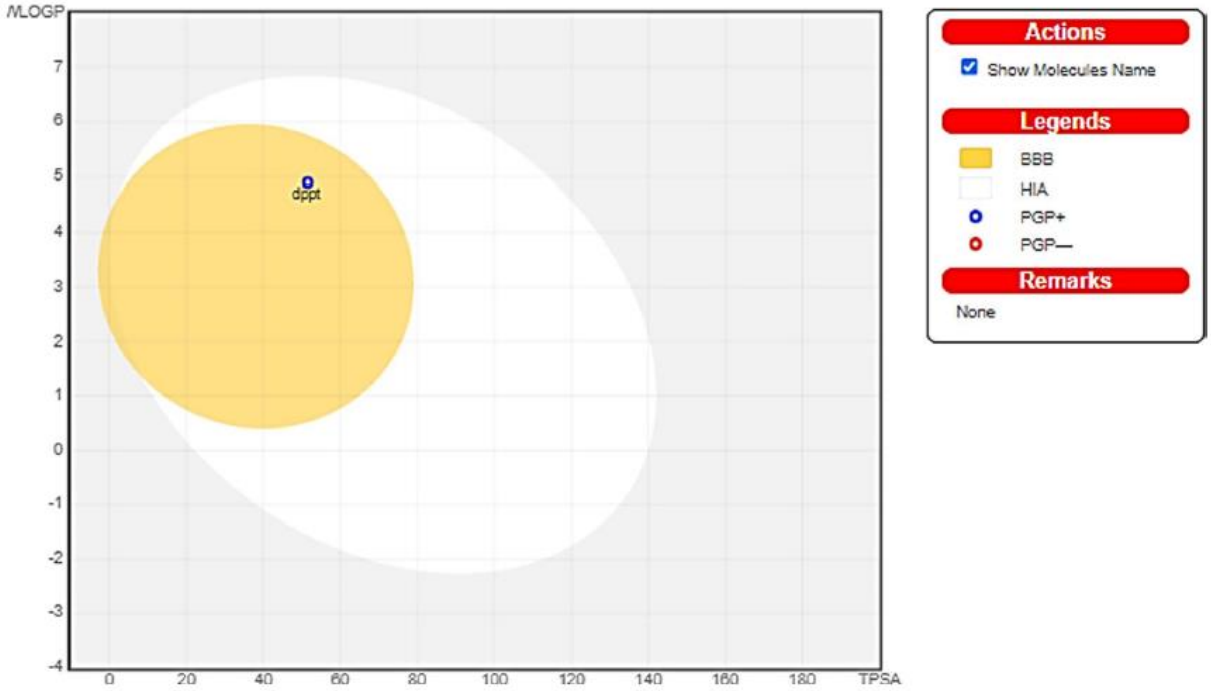

Fig. 14 Predicted BOILED-Egg diagram of the dppt ligand, from SwissADME web tool

Conclusions This article reports on the preparation of a cd(II) complex coordinated with two dppt ligands and in vitro studies of its inhibitory efects on cancerous human cell lines (MCF-7, U-87, and A549) as well as noncancerous cell line (NIH/3T3) through MTT assay and fow cytometric measurements, cellular DNA damage capability, DNA-binding afnity and DNA cleavage ability on a plasmid DNA (pUC19), in silico investigation of its afnity towards apoptosis relevant proteins

(APAF1, Bax, Bcl-2, Cas3, Cas7, and Cas9) and a model synthetic DNA, and ADME properties prediction using web-based SwissADME. In line with our previous evaluations of the biological activity of dppt-based metal complexes, herein we synthesized the [CdCl2(dppt)2] complex. The complex performed more efcient cytotoxic efects in MCF-7 cells than the other cells, U-87, A549, and NIH/3T3 in 24 h with IC50 values of 8.7, 18.2, 19.5, and 20.6 μM, respectively. Highly selective efect was found for the complex in MCF-7 cells at 10 and 20 μM concentrations over 24 h. The induced cell death in MCF-7 and U-87 cells after 24 h predominantly proceeded via apoptotic pathway as evidenced by the Annexin V-FITC/ PI assessment. The complex induced, in total, 37.89% apoptosis in MCF-7 and 33.66% in U-87 cells at 15 μM concentration, while the rates of necrotic death were 2.19% and 3.89%, respectively. The comet assay exhibited that the complex is capable to induce signifcant DNA damage in MCF-7 cells, which is further evidence of apoptosis. The complex interacted in vitro with DNA which was further evidenced by in silico studies to happen via partial intercalation. In contrast, the complex demonstrated potent DNA nuclease activity introducing it as a promising hydrolytic cleaving agent. In molecular docking free energy measurements, the complex docked with the chosen apoptotic proteins in the order of Bcl-2>APAF1>Bax> Cas9>Cas3>Cas7. This potential of the complex to interact with multiple modes of the apoptosis pathway with satisfactory scores (− 7.57 to − 9.25 kcal/mol) could be taken positively towards its high efcacy as a potential apoptosis inducer (Anighoro et al. 2014). Finally, ADME studies indicate that the complex has good ADME characteristics, notably in terms of the Veber rule and low GI absorption as well as signifcant biological activity.

Acknowledgements The authors would like to thank the Faculty of Pharmacy and Pharmaceutics Research Center, Kerman University of Medical Sciences, Kerman, Iran for their support. This study was approved by Kerman University of Medical Sciences with the research proposal number 400000640. **Author contributions** MA: Carrying out the experiments and writing the manuscript. MS: Carrying out the molecular docking studies. SJF: Synthesis data curation. SS: Carrying out MTT assay. AF: Flow cytometry data curation. BA: ADME studies, data curation, editing the manuscript, and supervising the whole work. Funding Not applicable. Data availability Not applicable. Code availability Not applicable. **Declarations**

Conflict of interest All authors declare no confict of interest.

Ethical approval This study was approved by the Research Ethics Committee of Kerman University of Medical Sciences, Kerman, Iran, with ethics code IR.KMU.REC.1400.414.

Consent to participate Not applicable.

Consent for publication All authors have read the final manuscript and declared consent for publication.

References

Abyar S, Khandar AA, Salehi R, Hosseini-Yazdi SA, Alizadeh E, Mahkam M, Jamalpoor A, White JM, Shojaei M, Aizpurua-Olaizola O, Masereeuw R, Janssen MJ (2019) In vitro nephrotoxicity and anticancer potency of newly synthesized cadmium complexes. Sci Rep 9:14686. https://doi.org/10.1038/s41598-019-51109-9

Ahamed M, Akhtar MJ, Khan MAM, Alhadlaq HA (2020) Reduced graphene oxide mitigates cadmium-induced cytotoxicity and oxidative stress in HepG2 cells. Food Chem Toxicol 143:111515. https://doi.org/10.1016/j.fct. 2020.111515

Ajibade PA, Fatokun AA, Andrew FP (2020) Synthesis, characterization and anti-cancer studies of Mn(II), Cu(II), Zn(II) and Pt(II) dithiocarbamate complexes - crystal structures of the Cu(II) and Pt (II) complexes. Inorg Chim Acta 504:119431. https://doi.org/10.1016/j.ica.2020.119431

Alalawy MD, Patel UH, Bhatt BS, Patel NJ (2020) Exploring qualitative and quantitative contributions of intermolecular interactions, DNA-binding and in vitro cytotoxic activity of isostructural and isomorphous Cd and Zn complexes. Polyhedron 185:114595. https://doi.org/10.1016/j. poly.2020.114595

Aljahdali MS, El-Sherif AA (2020) Synthesis and biological evaluation of novel Zn(II) and Cd(II) Schif base complexes as antimicrobial, antifungal, and antioxidant agents. Bioinorg Chem Appl 2020:1–17. https://doi.org/ 10.1155/2020/8866382

Anighoro A, Bajorath J, Rastelli G (2014) Polypharmacology: challenges and opportunities in drug discovery. J Med Chem 57:7874–7887. https://doi.org/10.1021/jm5006463

Anjomshoa M, Fatemi SJ, Torkzadeh-Mahani M, Hadadzadeh H (2014) DNA-and BSA-binding studies and anticancer activity against human breast cancer cells (MCF-7) of the zinc(II) complex

coordinated by 5,6-diphenyl-3-(2- pyridyl)-1,2,4-triazine. Spectrochim Acta Part A Mol Biomol Spectrosc 127:511–520. https://doi.org/10.1016/j.saa. 2014.02.048

Anjomshoa M, Hadadzadeh H, Fatemi SJ, Torkzadeh-Mahani M (2015a) A mononuclear Ni (II) complex with 5, 6-diphenyl3-(2-pyridyl)-1, 2, 4-triazine: DNA- and BSA-binding and anticancer activity against human breast carcinoma cells. Spectrochim Acta Part A Mol Biomol Spectrosc 136:205– 215. https://doi.org/10.1016/j.saa.2014.09.016

Anjomshoa M, Hadadzadeh H, Torkzadeh-Mahani M, Fatemi SJ, Adeli-Sardou M, Rudbari HA, Nardo VM (2015b) A mononuclear Cu(II) complex with 5, 6-diphenyl-3-(2- pyridyl)-1,2,4-triazine: synthesis, crystal structure, DNAand BSA-binding, molecular modeling, and anticancer activity against MCF-7, A-549, and HT-29 cell lines. Eur J Med Chem 96:66–82. https://doi.org/10.1016/j.ejmech. 2015.04.020

Anjomshoa M, Torkzadeh-Mahani M, Sahihi M, Rizzoli C, Ansari M, Janczak J, Sherafat Esfahani S, Ataei F, Dehkhodaei M, Amirheidari B (2019) Tris-chelated complexes of nickel(II) with bipyridine derivatives: DNA binding and cleavage, BSA binding, molecular docking, and cytotoxicity. J Biomol Struct Dyn 37:3887–3904. https://doi. org/10.1080/07391102.2018.1534700

Anjomshoa M, Amirheidari B (2022) Nuclease-like metalloscissors: biomimetic candidates for cancer and bacterial and viral infections therapy. Coord Chem Rev 458:214417. https://doi.org/10.1016/j.ccr.2022.214417

Arshad M, Bhat AR, Hoi KK, Choi I, Athar F (2017) Synthesis, characterization and antibacterial screening of some novel 1,2,4-triazine derivatives. Chin Chem Lett 28:1559– 1565. https://doi.org/10.1016/j.cclet.2016.12.037

Babgi BA, Mashat KH, Abdellattif MH, Arshad MN, Alzahrani KA, Asiri AM, Du J, Humphrey MG, Hussien MA (2020) Synthesis, structures, DNA-binding, cytotoxicity and molecular docking of CuBr (PPh3)(diimine). Polyhedron 192:114847. https://doi.org/10.1016/j.poly.2020.114847

Bhaskaran M, Devegowda VG, Gupta VK, Shivachar A, Bhosale RR, Arunachalam M, Vaishnavi T (2020) Current perspectives on therapies, including drug delivery systems, for managing

glioblastoma multiforme. ACS Chem Neurosci 11:2962–2977. https://doi.org/10.1021/acschemneuro.0c00555

Bhattacharyya MK, Dutta D, Nashre-ul-Islam SM, Frontera A, Sharma P, Verma AK, Das A (2020) Energetically signifcant antiparallel π-stacking contacts in Co(II), Ni(II) and Cu(II) coordination compounds of pyridine-2,6-dicarboxylates: antiproliferative evaluation and theoretical studies. Inorg Chim Acta 501:119233. https://doi.org/10.1016/j. ica.2019.119233

Bojarska J, Remko M, Breza M, Madura ID, Kaczmarek K, Zabrocki J, Wolf WM (2020) A supramolecular approach to structure-based design with a focus on synthons hierarchy in ornithine-derived ligands: review, synthesis, experimental and in silico studies. Molecules 25:1135. https:// doi.org/10.3390/molecules25051135

Bravo C, Robalo MP, Marques F, Fernandes AR, Sequeira DA, Piedade MFM, Garcia MH, de Brito MJV, Morais TS (2019) First heterobimetallic Cu(I)–dppf complexes designed for anticancer applications: synthesis, structural characterization and cytotoxicity. New J Chem 43:12308–12317. https://doi.org/10.1039/c9nj02068c

Bray F, Ferlay J, Soerjomataram I, Siegel RL, Torre LA, Jemal A (2018) Global cancer statistics 2018: GLOBOCAN estimates of incidence and mortality worldwide for 36 cancers in 185 countries. CA Cancer J Clin 68:394–424. https://doi.org/10.3322/caac.21492

Cascioferro S, Parrino B, Spanò V, Carbone A, Montalbano A, Barraja P, Diana P, Cirrincione G (2017) An overview on the recent developments of 1,2,4-triazine derivatives as anticancer compounds. Eur J Med Chem 142:328–375. https://doi.org/10.1016/j.ejmech.2017.08.009

Chen Z, Wu Y, Zhu Z, Zhang Y (2019) DNA cleavage, DNA/ HSA binding study, and antiproliferative activity of a phenolate-bridged binuclear copper(II) complex. Biometals 32:227–240. https://doi.org/10.1007/s10534-019-00172-w

Daina A, Zoete V (2016) A boiled-egg to predict gastrointestinal absorption and brain penetration of small molecules. ChemMedChem 11:1117–1121. https://doi.org/10.1002/ cmdc.201600182

Daina A, Blatter MC, Gerritsen VB, Palagi PM, Marek D, Xenarios I, Schwede T, Michielin O, Zoete V (2017a) Drug design workshop: a web-based educational tool to introduce computer-aided

drug design to the general public. J Chem Educ 94:335–344. https://doi.org/10.1021/acs.jchemed.6b00596

Daina A, Michielin O, Zoete V (2017b) SwissADME: a free web tool to evaluate pharmacokinetics, drug-likeness and medicinal chemistry friendliness of small molecules. Sci Rep 7:1–13. https://doi.org/10.1038/srep42717

Desbouis D, Troitsky IP, Belousof MJ, Spiccia L, Graham B (2012) Copper(II), zinc(II) and nickel(II) complexes as nuclease mimetics. Coord Chem Rev 256:897–937. https://doi.org/10.1016/j.ccr.2011.12.005

Dutta D, Sharma P, Frontera A, Gogoi A, Verma AK, Dutta D, Sarma B, Bhattacharyya MK (2020) Oxalato bridged coordination polymer of manganese(III) involving unconventional O···π-hole(nitrile) and antiparallel nitrile···nitrile contacts: antiproliferative evaluation and theoretical studies. New J Chem 44:20021–20038. https:// doi.org/10.1039/D0NJ03712E

Fang Y, Li J, Han PP, Han QX, Li MX (2018) Less toxic zinc (II), diorganotin (IV), gallium (III) and cadmium (II) complexes derived from 2-benzoylpyridine N,N-dimethylthiosemicarbazone: synthesis, crystal structures, cytotoxicity and investigations of mechanisms of action. Toxicol Res 7:987–993. https://doi.org/10.1039/c8tx00127h

Fathima SSA, Paulpandiyan R, Nagarajana ER (2018) Expatiating biological excellence of aminoantipyrine derived novel metal complexes: combined DNA interaction, antimicrobial, free radical scavenging studies and molecular docking simulations. J Mol Struct 1178:179–191. https:// doi.org/10.1016/j.molstruc.2018.10.021

Gitarić J, Stanojević IM, Rodić MV, Drašković NS, Stevanović M, Vojnović S, Djuran MI, Glišić BĐ (2020) Structural characterization and biological evaluation of polynuclear Mn(II) and Cd(II) complexes with 2, 2-dimethyl-1, 3-propanediamine-N, N, N', N'-tetraacetate The infuence of ligand structure and counter cation on the complex nuclearity. Polyhedron 188:114688. https://doi.org/10.1016/j. poly.2020.114688

Gogoi A, Das A, Frontera A, Verma AK, Bhattacharyya MK (2019) Energetically signifcant unconventional π-π contacts involving fumarate in a novel coordination polymer of Zn(II): In-vitro

anticancer evaluation and theoretical studies. Inorg Chim Acta 493:1–13. https://doi.org/10.1016/j.ica.2019.04.047

Guan QL, Liu Z, Wei WJ, Xing YH, Liu J, Zhang R, Hou YN, Wang X, Bai FY (2014) Synthesis, structure, spectroscopy of four novel supramolecular complexes and cytotoxicity study by application of multiple parallel perfused microbioreactors. New J Chem 38:3258–3268. https://doi.org/10.1039/c3nj01646c

Ibrahim AO, Zhou Y, Jiang F, Chen L, Li X, Xu W, Onawumi OO, Odunola OA, Hong M (2011) An unusual (10,3)-d MOF material with nanoscale helical cavities and multifunctionality. Eur J Inorg Chem 2011:5000–5005. https:// doi.org/10.1002/ejic.201100566

Jeyalakshmi K, Haribabu J, Balachandran C, Bhuvanesh NSP, Emi N, Karvembu R (2017) Synthesis of Ru(II)–benzene complexes containing aroylthiourea ligands, and their binding with biomolecules and in vitro cytotoxicity through apoptosis. New J Chem 41:2672–2686. https://doi.org/10.1039/c6nj03099h

Jin Y, Cowan JA (2005) DNA cleavage by copper-ATCUN complexes. Factors infuencing cleavage mechanism and linearization of dsDNA. J Am Chem Soc 127:8408–8415. https://doi.org/10.1021/ja0503985.s001

Khan T, Ahmad R, Azad I, Raza S, Joshi S, Khan AR (2018) Computer-aided drug design and virtual screening of targeted combinatorial libraries of mixed-ligand transition metal complexes of 2-butanone thiosemicarbazon. Comput Biol Chem 75:178–195. https://doi.org/10.1016/j.compbiolchem.2018.05.008

Khandar AA, Azar ZM, Eskandani M, Hubschle CB, van Smaalen S, Shaabani B, Omidi Y (2019) Cadmium(II) complexes of a hydrazone ligand: synthesis, characterization, DNA binding, cyto- and genotoxicity studies. Polyhedron 171:237–248. https://doi.org/10.1016/j.poly.2019.06. 026

Korkmaz N, Karadağ A, Aydın A, Yanar Y, Karaman İ, Tekin Ş (2014) Synthesis and characterization of two novel dicyanidoargentate(I) complexes containing N-(2-hydroxyethyl) ethylenediamine exhibiting signifcant biological activity. New J Chem 38:4760–4773. https://doi.org/10. 1039/c4nj00851k

L'Azou B, Passagne I, Mounicou S, Tréguer-Delapierre M, Puljalté I, Szpunar J, Lobinski R, Ohayon-Courtès C (2014) Comparative cytotoxicity of cadmium forms (CdCl2, CdO, CdS micro- and nanoparticles) in renal cells. Toxicol Res 3:32–41. https://doi.org/10.1039/c3tx50063b

Li J, Huang WY, Qian SS, Li QY, Zhu HL (2015a) Two novel 2D waves copper(II) coordination polymer with the quinolone antimicrobial drugs ciprofoxacin: synthesis, structure and biological evaluation. Inorg Chim Acta 435:16– 24. https://doi.org/10.1016/j.ica.2015.06.001

Li F, Xie J, Feng F (2015b) Copper and zinc complexes of a diaza-crown ether as artifcial nucleases for the efcient hydrolytic cleavage of DNA. New J Chem 39:5654–5660. https://doi.org/10.1039/c4nj02193b

Li J, Liu R, Jiang J, Liang X, Huang G, Yang D, Chen H, Pan L, Ma Z (2020) Synthesis, characterization, photoluminescence, antiproliferative activity, and DNA interaction of cadmium(II) substituted 4′-phenyl-terpyridine compounds. J Inorg Biochem 210:111165. https://doi.org/10.1016/j.jinorgbio.2020.111165

Liu P, Liu J, Zhang YQ, Wu BY, Wang KZ (2015) Synthesis, DNA binding and photocleavage, and cellular uptake of an alkyl chain-linked dinuclear ruthenium (II) complex. J Photochem Photobiol B Biol 143:89–99. https://doi.org/ 10.1016/j.jphotobiol.2015.01.004

Lopes J, Alves D, Morais TS, Costa PJ, Piedade MFM, Marques F, de Brito MJV, Garcia MH (2017) New copper(I) and heteronuclear copper(I)–ruthenium(II) complexes: synthesis, structural characterization and cytotoxicity. J Inorg Biochem 169:68–78. https://doi.org/10.1016/j.jinorgbio.2017.01.007

Lopes ED, Oliveira CG, Silva PB, Eismann CE, Suárez CA, Menegário AA, Leite CQF, Defon VM, Pavan FR (2016) Novel zinc(II) complexes [Zn(atc-Et)2] and [Zn(atc-Ph)2]: in vitro and in vivo antiproliferative studies. Int J Mol Sci 17:781. https://doi.org/10.3390/ijms1 7050781

Luo HY, Li JY, Li Y, Zhang L, Li JY, Jia DZ, Xu GC (2016) Cadmium(II) complexes with a 4-acyl pyrazolone derivative and co-ligands: crystal structures and antitumor activity. RSC Adv 6:114997–115009. https://doi.org/10.1039/ c6ra23938b

Ma Y, Rivera-Ingraham G, Nommick A, Bickmeyer U, Roeder T (2020) Copper and cadmium administration induce toxicity and oxidative stress in the marine fatworm Macros- tomum lignano. Aquat Toxicol 221:105428. https://doi. org/10.1016/j.aquatox.2020.105428

Machura B, Świtlicka A, Kruszynski R, Mroziński J, Kłak J, Kusz J (2008) Coordination studies of 5,6-diphenyl-3-(2- pyridyl)-1,2,4-triazine towards Cu2+ cation. X-ray studies, spectroscopic characterization and DFT calculations. Polyhedron 27:2959–2967. https://doi.org/10.1016/j.poly.2008.05.033

Majumdar D, Biswas JK, Mondal M, Babu MSS, Das S, Metre RK, SreeKumar SS, Bankura K, Mishra D (2018) Cd(II) pseudohalide complexes with N, N′-bis (3-ethoxysalicylidenimino) 1, 3-diaminopropane: crystal structures, hirshfeld surface, antibacterial and anti-bioflm properties. ChemistrySelect 3:2912–2925. https://doi.org/10.1002/ slct.201702970

Manikandan R, Chitrapriya N, Jang YJ, Viswanathamurthi P (2013) Evaluation of DNA-binding, radical scavenging and cytotoxic activity of fve coordinated Cd(II) complexes containing 2-acetylpyridine-N 4-substituted thiosemicarbazone. RSC Adv 3:11647–11657. https://doi.org/10.1039/c3ra40814k

Marandi F, Fun HK, Quah CK (2011) Synthesis of new complexes of cadmium(II) with 3-(2-Pyridyl)-5, 6-diphenyl-1,2,4-triazine ligand: study of the efect of weak interactions on their crystal packing. Synth React Inorg M 41:234–240. https://doi.org/10.1080/15533174.2011. 555852

Martínez MÁ, Carranza MP, Massaguer A, Santos L, Organero JA, Aliende C, de Llorens R, Ng-Choi I, Feliu L, Planas M, Rodríguez AM, Manzano BR, Espino G, Jalón FA (2017) Synthesis and biological evaluation of Ru(II) and Pt(II) complexes bearing carboxyl groups as potential anticancer targeted drugs. Inorg Chem 56:13679–13696. https://doi.org/10.1021/acs.inorgchem.7b01178

Matos CP, Adiguzel Z, Yildizhan Y, Cevatemre B, Onder TB, Cevik O, Nunes P, Ferreira LP, Carvalho MD, Campos DL, Pavan FR, Pessoa JC, Garcia MH, Tomaz AI, Correia I, Acilan C (2019) May iron(III) complexes containing phenanthroline derivatives as ligands be prospective anticancer agents? Eur J Med Chem 176:492–512. https:// doi.org/10.1016/j.ejmech.2019.04.070

Mishra A, Dey S (2019) Molecular docking studies of a cyclic octapeptide-cyclosaplin from sandalwood. Biomolecules 9:740. https://doi.org/10.3390/biom9110740

Mlejnek P, Dolezel P, Maier V, Kikalova K, Skoupa N (2019) N-acetylcysteine dual and antagonistic efect on cadmium cytotoxicity in human leukemia cells. Environ Toxicol Pharmacol 71:103213. https://doi.org/10.1016/j.etap. 2019.103213

Morgan SM, El-Sonbati AZ, Eissa HR (2017) Geometrical structures, thermal properties and spectroscopic studies of Schif base complexes: correlation between ionic radius of metal complexes and DNA binding. J Mol Liq 240:752– 776. https://doi.org/10.1016/j.molliq.2017.05.114

Morris GM, Goodsell DS, Halliday RS, Huey R, Hart WE, Belew RK, Olson AJ (1998) Automated docking using a Lamarckian genetic algorithm and an empirical binding free energy function. J Comput Chem 19:1639–1662. https://doi.org/10.1002/(sici)1096-987x(19981115)19:14%3c1639::aid-jcc10%3e3.0.co;2-b

Mosmann T (1983) Rapid colorimetric assay for cellular growth and survival: application to proliferation and cytotoxicity assays. J Immunol Methods 65:55–63. https://doi.org/10.1016/0022-1759(83)90303-4

Nath H, Dutta D, Sharma P, Frontera A, Verma AK, BarcelóOliver M, Devi M, Bhattacharyya MK (2020) Adipato bridged novel hexanuclear Cu(II) and polymeric Co(II) coordination compounds involving cooperative supramolecular assemblies and encapsulated guest water clusters in square grid host: antiproliferative evaluation and theoretical studies. Dalton Trans 49:9863–9881. https://doi. org/10.1039/D0DT01007C

Nath H, Sharma P, Gomila RM, Frontera A, Barceló-Oliver M, Verma AK, Dutta K, Bhattacharyya MK (2021) Unconventional enclathration of guest adipic acid and energetically signifcant antiparallel π-stacked ternary assemblies involving unusual regium- π(chelate) contacts in phenanthroline-based Ni(II) and Cu(II) compounds—antiproliferative evaluation and theoretical studies. J Mol Struct 1245:131038. https://doi.org/10.1016/j.molstruc.2021. 131038

Qazi SU, Rahman SU, Awan AN, al-Rashida M, Alharthy RD, Asari A, Hameed A, Iqbal J (2018) Semicarbazone derivatives as urease inhibitors: synthesis, biological evaluation, molecular

docking studies and in-silico ADME evaluation. Bioorg Chem 79:19–26. https://doi.org/10.1016/j.bioorg.2018.03.02

Rukk NS, Kuzmina LG, Shamsiev RS, Davydova GA, Mironova EA, Ermakov AM, Buzanov GA, Skryabina AY, Streletskii AN, Vorob'eva GA, Retivov VM, Volkov PA, Belus SK, Kozhukhova EI, Krasnoperova VN (2019) Zinc (II) and cadmium (II) halide complexes with cafeine: synthesis, X-ray crystal structure, cytotoxicity and genotoxicity studies. Inorg Chim Acta 487:184–200. https://doi.org/10.1016/j.ica.2018.11.036

Sharma P, Dutta D, Gomila RM, Frontera A, Barcelo-Oliver M, Verma AK, Bhattacharyya MK (2021) Benzoato bridged dinuclear Mn(II) and Cu(II) compounds involving guest chlorobenzoates and dimeric paddle wheel supramolecular assemblies: antiproliferative evaluation and theoretical studies. Polyhedron 208:115409. https://doi. org/10.1016/j.poly.2021.115409

Spel L, Boelens JJ, Nierkens S, Boes M (2013) Antitumor immune responses mediated by dendritic cells: how signals derived from dying cancer cells drive antigen crosspresentation. OncoImmunology 2:e26403. https://doi.org/ 10.4161/onci.26403

Tsave O, Iordanidou C, Gabriel C, Hatzidimitriou A, Salifoglou A (2019) Binary-ternary Cd (II)-(hydroxycarboxylic acid)-(aromatic chelator) systems exhibit in vitro cytotoxic selectivity in a tissue-specifc manner. J Inorg Biochem 195:201–215. https://doi.org/10.1016/j.jinorgbio.2019.02.009

Wang B, Wang H, Han D, Chen J, Yin Y (2020) Studying the mixture efects of brominated fame retardants and metal ions by comet assay. Environ Pollut 267:115677. https://doi.org/10.1016/j.envpol.2020.115677

Yamada A, Mabe T, Yamane R, Noda K, Wasada Y, Inamo M, Ishihara K, Suzuki T, Takagi HD (2015) Flipping of the coordinated triazine moiety in Cu(I)–L2 and the small electronic factor, κel, for direct outer-sphere cross reactions: syntheses, crystal structures and redox behaviour of copper (II)/(I)–L2 complexes (L= 3-(2-pyridyl)-5, 6-diphenyl-1, 2, 4-triazine). Dalton Trans 44:13979–13990. https://doi.org/10.1039/c5dt01808k

Zhang N, Fan Y, Huang G, Buac D, Bi C, Ma Y, Wang X, Zhang Z, Zhang X, Dou QP (2017) l-tryptophan Schif base cadmium(II) complexes as a new class of proteasome inhibitors and

apoptosis inducers in human breast cancer cells. Inorg Chim Acta 466:478–485. https://doi.org/10.1016/j.ica.2017.07.006

Zhang HB, Zhang XF, Chai LQ, Tang LJ, Zhang HS (2020) Zinc(II) and cadmium(II) complexes containing imidazole ring: structural, spectroscopic, antibacterial, DFT calculations and Hirshfeld surface analysis. Inorg Chim Acta 507:119610. https://doi.org/10.1016/j.ica.2020.119610

Zhao J, Peng K, Guo Y, Zhang J, Chen S, Hu J (2015) Photoluminescent and cytotoxic properties of multinuclear complexes and multinuclear-based polymers with group 12 metals and tripodal ligand. New J Chem 39:6016–6024. https://doi.org/10.1039/C5NJ00222B

Zvirzdinaite M, Garbe S, Arefyeva N, Krause M, von der Stück R, Klein A (2017) Palladium(II) complexes of ambidentate and potentially cyclometalating 5-aryl-3-(2′-pyridyl)- 1,2,4-triazine ligands. Eur J Inorg Chem 2017:2011–2022. https://doi.org/10.1002/ejic.201601530